

*Invited paper***Theory and design of chirped dielectric laser mirrors****R. Szipőcs^{1,2}, A. Kóházi-Kis²**¹Research Institute for Solid State Physics, P.O. Box 49, H-1525 Budapest, Hungary²R&D Lézer-Optika Bt, P.O. Box 622, H-1539 Budapest, Hungary

Received: 11 March 1997/Revised version: 26 April 1997

Abstract. Chirped dielectric laser mirrors offer a general solution for broadband feedback and dispersion control in femtosecond laser systems. Chirped mirrors developed for mode-locked solid-state lasers, femtosecond parametric oscillators, chirped pulse amplification systems and pulse compressors are introduced. Basic theoretical and design considerations are also presented.

PACS: 42.15.Eq; 42.25.Bs; 42.40.Pa; 42.60.Da; 42.65.k; 42.79.Bh; 42.80.V

One of the main trends of laser physics today is ultrafast laser technology. Recent research on high-power semiconductor laser diodes and solid-state laser materials with a broad fluorescence emission band has paved the way for compact, reliable, broadly tunable all-solid-state continuous wave (cw), picosecond (ps) and femtosecond (fs) pulse laser sources. One approach is based on Ti:sapphire (Ti:S) [1], which can be efficiently pumped by the frequency-doubled output of AlGaAs diode-pumped neodymium lasers. Alternatively, the direct diode pumping of colquirrite laser-active materials such as LiCaAlF₆:Cr³⁺ (Cr:LiCAF) [2], LiSrAlF₆:Cr³⁺ (Cr:LiSAF) [3], and LiSrGaF₆:Cr³⁺ (Cr:LiSGAF) [4] became feasible by the use of enhanced mode-matching schemes [5] or AlGaInP semiconductor lasers with “improved” beam quality operating near 670 nm [6]. The latter approach might offer greater simplicity, efficiency, compactness, and cost effectiveness. The importance of these features for wide-ranging applications needs no explanation. These advances in laser technology offered the possibility of constructing laser oscillators generating optical pulses in the sub-20-fs regime by using different mode-locking techniques such as self-mode-locking of the laser [7].

Because of the dominant role of soliton-like pulse shaping in ultrashort-pulse solid-state lasers [8], femtosecond-pulse generation relies on net negative, i.e. anomalous, intracavity group-delay dispersion (GDD). Solid-state gain media always introduce a certain amount of frequency-dependent positive (normal) dispersion in the cavity, which must be balanced as

well. Until recently, Brewster-angled prism pairs [9] built into the laser cavity were the only low-loss sources of broadband negative GDD. In prism-pair-controlled broadband lasers, a major limitation to ultrashort-pulse generation originates from the variation of the intracavity GDD with wavelength. The principal source of this higher-order dispersion, however, was found to be the prism pair [10, 11]. If the lasers are operated in the vicinity of zero GDD, the spectra of sub-20-fs pulses from prism-pair-controlled oscillators are asymmetric with a broad shoulder [10] or are double peaked [8, 11] depending on whether the soliton-like pulses are, respectively, third- or fourth-order dispersion limited. This deviation from the ideal sech pulse spectrum causes a weak but significant pedestal in the time domain, the length of which may substantially exceed the pulse duration defined as the full width at half maximum (FWHM) intensity. This degradation in pulse quality may be unacceptable in a number of spectroscopic applications requiring high temporal resolution. An additional problem in the time domain is the increased sensitivity of the pulse width to the cavity and prism alignment. Cavity mirror alignment changes the position of the resonator axis and thus the glass path through the prisms. Hence any small cavity realignment calls for subsequent readjustment of the prism positions and orientation to restore the original pulse width and the corresponding spectrum. This makes “turn-key” operation and thus the integration of these devices in complex systems [e.g. chirped pulse amplification (CPA) systems, opto-electronic data processing systems] extremely difficult. Furthermore, the minimum prism separation sets a constraint on the resonator length and, in turn, the size and repetition rate of femtosecond-pulse solid-state laser oscillators.

Continuous wave, ps, and fs lasers contain optical coatings as important functional elements, e.g., high reflectors (HR), output couplers (OC), and antireflection (AR) coatings. These optical elements are based on the interference phenomenon of light. Their theoretical analysis generally relies on the well-known scattering matrix formalism [12, 13] derived from the Maxwell equations. Laser performance strongly depends on the quality of optical coatings: the high reflectors

tors should approach the ideal 100% reflectance at the operation wavelengths in order to minimize intracavity losses; the output coupling has to be set to specific values to ensure optimum operation. In broadband mode-locked or broadly tunable laser systems, broadband intracavity and extracavity mirrors covering possibly the whole fluorescence spectrum of the laser active medium are needed; the reflectivity of such mirrors is not determined solely at the operation wavelengths but at the pump wavelength(s) as well. *In the particular case of femtosecond laser systems, all the coatings must also be designed for phase characteristics to prevent the pulse shape from undesirable distortion.*

In the case of high reflectors, a combination of materials with the highest refractive-index ratios (n_H/n_L) is usually preferred since the higher the ratio, the higher the theoretical reflectance and bandwidth of standard quarterwave stacks. Among its competitors, the $\text{TiO}_2/\text{SiO}_2$ pair has the highest ratio over the near-infrared spectral range [14]. In the production of a high-density coating with low scattering and absorption losses, ion-based technologies could be advantageous [15]. However, the total number of layers is strictly limited by the relatively high stress in such coatings, which does not allow the deposition of dielectric mirrors formed by a relatively high number of thick layers in the near infrared. At the optical coating laboratory of the Research Institute for Solid State Physics, Budapest, Hungary, a BAK 550 box coater supplied with an ESQ 110 electron beam gun (products from Balzers AG) is used for depositing laser optical coatings. Our unconventional coating deposition technology (called reactive electron beam deposition under reduced oxygen pressure), results in relatively high density optical coatings of the $\text{TiO}_2/\text{SiO}_2$ and $\text{Ta}_2\text{O}_5/\text{SiO}_2$ material pairs with low absorption and scattering losses. For details on all of these, see [14]. In the case of Ti:sapphire lasers, for instance, the useful bandwidth of our low-dispersion quarterwave mirrors made of $\text{TiO}_2/\text{SiO}_2$ is limited to approximately 180 nm around 800 nm [14]. *In addition to the high-order dispersion existing in prism-pair-controlled fs laser systems, the bandwidth of low-dispersion dielectric mirrors forming the laser cavity appeared to be the main limiting factor for obtaining optical pulses below 10 fs, directly from a laser oscillator.*

The problem of designing broadband dielectric mirrors for sub-10-fs or broadly tunable femtosecond solid-state laser systems is twofold. First, the mirrors have to have *continuous high reflectivity over a broad spectral range* without any drop in reflectivity regardless of wavelength. Second, the mirrors have to exhibit a *smooth, possibly negative variation of the group delay vs. frequency function over the whole operation range*, allowing femtosecond mode-locked operation of the laser. It is worth mentioning here that these two requirements can be fulfilled by properly designed metallic mirrors; however, their reflectivity is considerably lower than that of a dielectric mirror and therefore they usually cannot be used as intracavity broadband mirrors in femtosecond laser oscillators. Previously proposed solutions to extend the high reflectivity range of dielectric mirrors, such as (i) deposition of low-pass (high-pass) stacks as a single coating [16], and (ii) deposition of multilayer stacks with variation of thickness in arithmetic or geometric progression [17], do not meet the above-mentioned requirements (for details of all of these, see [14, 18–20]). Briefly, all of the previously used broadband dielectric mirrors exhibited rapid change of the reflected

phase at specific wavelengths in the high-reflectivity zone of the broadband mirrors, causing resonant losses [18] and extremely strong high-order dispersions [19, 20] around these wavelengths, thus preventing their use in broadly tunable femtosecond oscillators [14].

In this paper we discuss a novel technology for ultrashort-pulse generation that uses what have become known as *chirped dispersive dielectric mirrors*, or *chirped mirrors* [21, 22]. These special laser mirrors, which are potentially free from all the drawbacks listed above, can be used for broadband feedback, intracavity and extracavity dispersion control. In the following, special laser mirror designs exhibiting high reflectivity and negative GDD over broad frequency ranges are shown. The design technique, deposition technology, and quality control permit higher-order contributions to the mirror phase dispersion to be kept low or to be chosen such that high-order phase errors introduced by other system components (e.g., the gain medium, prism pairs) are cancelled. By replacing conventional thin-film optics (and prism pairs in most of the cases), these novel devices made a Kerr-lens mode-locked, solid-state lasers more feasible. These lasers deliver nearly bandwidth-limited 7.5-fs pulses from Ti:sapphire lasers [23–25] around 0.8 μm , and sub-20-fs pulses from Cr:LiSAF and Cr:LiSGaF [26, 27] lasers at around 840 nm. In addition, the use of chirped mirrors simplifies the cavity design and permits the construction of compact, reliable, high-output-power (and high-repetition-rate) sub-20-fs sources as well. Further applications of chirped mirrors that have already been accomplished include, for example, using them for broadband feedback and dispersion control in broadly tunable cw, ps, and fs solid-state lasers [28] and parametric oscillators [29, 30]; broadband third- and fourth-order dispersion control in pulse compression schemes used in CPA systems [31–33]; or in white-light-continuum compression experiments [34] supporting pulses below 5 fs [35, 36].

First we present theoretical considerations of the operation of chirped dielectric laser mirrors. We point out the analogy between the holography of wave packets in a volume medium [37] and our chirped mirrors. Based on our theoretical considerations, formulae are presented that can be efficiently utilized to synthesize *graded-index* dielectric mirrors with prescribed dispersion properties. Next we deal with chirped mirrors consisting of alternate *discrete* layers of TiO_2 and SiO_2 ; we present general and particular design considerations for different application problems and we also discuss in detail the method of construction. Representative dispersive mirror designs developed for different femtosecond-pulse solid-state lasers, parametric oscillators, CPA systems and pulse compressors are then shown. By computing the electric-field distribution inside the dielectric mirrors (built of discrete layers) as a function of the wavelength, we derive their dispersive properties from the wavelength dependence of the penetration depth of the incident optical field in accordance with our theoretical considerations. There are some important technological issues that must be taken into account during the design of chirped mirrors: reflection losses and sensitivity to deposition errors. Based on our atomic-force-microscopy (AFM) and reflectivity measurements, reflection losses at chirped mirrors made by different technologies are compared. The second technological issue that must be mentioned is the fact that dispersive properties of chirped mir-

rors exhibit a relatively high sensitivity to deposition errors in the layer thickness. This technological problem could be efficiently eliminated by developing rapid, accurate, inexpensive methods for dispersion measurement on laser mirrors. Measured GDD versus wavelength functions of accomplished dispersive mirrors are presented. These data were obtained by using different interferometric arrangements combined with a spectrograph [38, 39]. Finally, some typical applications of chirped mirror technology are presented.

1 Theory

As a starting point, an analogy between *chirped dielectric laser mirrors* and *one-dimensional (1D) phase-volume holograms* written by two counter-propagating (chirped) laser pulses [37] is established. We show that chirped mirrors can be regarded as artificial, 1D holograms exhibiting extremely high, sudden refractive-index modulations and relatively small overall thicknesses. In femtosecond laser cavities, the most important requirement is to have minimum losses in the cavity over the whole operation range; this requirement can be fulfilled by properly designed (chirped) dielectric mirrors only. However, in pulse stretcher and compression schemes developed for CPA systems [31–33], or in white-light-continuum compression experiments [34–36], proper dispersion control over the whole spectrum is of primary importance. In the latter case, one can tolerate considerably higher losses than in intracavity applications. One of the possible promising solutions for the problem of pulse stretching and compression in CPA systems was recently presented by Loiseaux et al. [40], who used a pair of *chirped transmission gratings* placed perpendicularly to each other to provide an almost linear time delay versus frequency function.

The main disadvantage of volume holograms written by short light pulses is their low diffraction efficiency because of the low refractive-index modulation, the high bias exposure, and the short physical length of the interference pattern. It is worth mentioning that the experimental realization of the idea of pulse shaping in phase-volume holograms has been recently performed by Hill and Brady [41] for instance. However, the reflectivity of the phase-volume hologram can be considerably increased by dispersing the frequency components in space for recording the interference pattern, which is called *spectral holography* [37, 42]. The potential applications of spectral holography for broadband dispersion compensation have been presented in [37, 42]. In Sect. 1.2, we briefly conclude the main results in connection with *broadband dispersion compensation* and *time-reversal of femtosecond laser pulses* and mention our preliminary experimental results on phase conjugation in a photorefractive medium [43]. Sect. 1.3 presents analytical formulae derived from the analogy between chirped mirrors and volume reflection holograms. The formulae can be used to *synthesize graded-index chirped mirrors with prescribed dispersion properties*. Though these formulae do not directly result in high-reflectivity laser mirrors built of discrete layers, they do help us to gain a better understanding of the operation of chirped mirrors, and they do provide a route towards starting designs made of discrete layers and physically correct coating design specifications for further optimization. Note, however, that these graded-index (or

rugate) chirped mirrors could also be manufactured via different, state-of-the-art optical coating deposition techniques.

1.1 Holography of wave packets

In the following, we show that the interference pattern formed by two counter-propagating (Gaussian) pulses exhibiting different chirp parameters are capable of forming “chirped mirrors” in a holographic (or photorefractive) medium with the assumption that the local change in the refractive index is proportional to the exposure in the phase-volume hologram. If one of the pulses (reference) is chirp free (i.e., dispersion free; $\tau(\omega)$ is constant at any x position), the interference pattern records the temporal structure (chirp) of the signal pulse in the spatial domain. After recording such an interference pattern in a volume holographic medium, the chirp of the signal pulse is almost perfectly compensated when it is reflected on the corresponding (spatially chirped) hologram, i.e., a nearly *ideal graded index chirped mirror* for dispersion compensation is constructed.

The following calculations are based on the theoretical paper by Mazurenko [37]. Our calculations are restricted, however, to investigating the one-dimensional spatial structure of the recorded phase-volume hologram in the particular case in which the hologram is written by two counter-propagating laser pulses.

Let us consider two Gaussian light pulses, one of them being dispersion free and the other being linearly chirped, with dimensionless (linear) chirp parameters $a_1 = a \neq 0$ and $a_2 = 0$. The time-dependent electric field of the pulses can be written as

$$E_k(t) = E_{0,k} \exp\left(-\frac{t^2}{2T_k^2}\right) \cos\left(\omega_0 t + a_k \frac{t^2}{T_k^2}\right), \quad (1)$$

where T_k is defined as the half width at $1/e$ maximum intensity time duration, $E_{0,k}$ is the electric field amplitude of the k th light pulse ($k = 1, 2$), and ω_0 is the (common) central frequency of the two pulses.

We investigate a practical situation in which the two light pulses exhibit the same $\Delta\omega$ spectral bandwidth. With the notation T_0 for the transform-limited pulse duration ($T_0 = 1/\Delta\omega$), the pulse duration T_k and the group-delay dispersion (GDD = $\partial^2\varphi/\partial\omega^2$) parameter, D_k , of the k th light pulse can be expressed as

$$T_k = T_0 \left(1 + 4a_k^2\right)^{1/2} = T_0 \left(1 + \frac{D_k^2}{T_0^4}\right)^{1/2}, \quad (2)$$

$$D_k = 2a_k T_0^2 = \frac{2a_k T_k^2}{1 + 4a_k^2}. \quad (3)$$

We consider the particular case in which the two pulses are propagating in opposite directions along the x axis (in one dimension). The temporal and spatial dependences of the electric field can be written as

$$E_1(t, x) = E_1\left(t - \frac{x}{c}\right) \quad \text{and} \quad E_2(t, x) = E_2\left(t + \frac{x}{c}\right). \quad (4)$$

The time-averaged intensity distribution along the x axis, $P(x)$, can be calculated as

$$P(x) = \int_{-\infty}^{\infty} \left[E_1 \left(t - \frac{x}{c} \right) + E_2 \left(t + \frac{x}{c} \right) \right]^2 dt. \quad (5)$$

After expansion we obtain

$$P(x) = \int_{-\infty}^{\infty} \left[E_1 \left(t - \frac{x}{c} \right)^2 + E_2 \left(t + \frac{x}{c} \right)^2 + 2E_1 \left(t - \frac{x}{c} \right) E_2 \left(t + \frac{x}{c} \right) \right] dt. \quad (6)$$

By transforming the t variable inside the integral in the first two terms we get

$$P(x) = \int_{-\infty}^{\infty} \left[E_1(t)^2 + E_2(t)^2 \right] dt + 2 \int_{-\infty}^{\infty} E_1 \left(t - \frac{x}{c} \right) E_2 \left(t + \frac{x}{c} \right) dt. \quad (7)$$

We can transform the t variable also in the second integral of (7):

$$P(x) = \int_{-\infty}^{\infty} \left[E_1(t)^2 + E_2(t)^2 \right] dt + 2 \int_{-\infty}^{\infty} E_1(t) E_2 \left(t + \frac{2x}{c} \right) dt. \quad (8)$$

The second integral in (8) is the convolution of the electric field functions defined in (1):

$$K(x) = \int_{-\infty}^{\infty} E_1(t) E_2 \left(t + \frac{2x}{c} \right) dt = \left[E_1(t) * E_2(-t) \right] \Big|_{-2x/c}. \quad (9)$$

In (9) the $*$ sign denotes convolution.

To calculate the convolution in (9) we take the Fourier transform of the E_k electric field functions. Then we multiply the Fourier transforms and take the inverse Fourier transform of the product. This procedure is well known from convolution theory. The Fourier spectra of the two pulses are composed of positive and negative frequency components. If we take the product of the two spectra, cross-products of the negative and positive components can be neglected in practical cases. Finally, we come to the following formula:

$$K(x) = \frac{1}{4} E_{0,1} E_{0,2} T_0 \sqrt{\pi} \left(\frac{1+4a^2}{1+a^2} \right)^{1/4} \exp \left(-\frac{x^2}{c^2 T_0^2 (1+a^2)} \right) \times \cos \left(2k_0 x - \frac{ax^2}{c^2 T_0^2 (1+a^2)} - \varphi \right), \quad (10)$$

where k_0 denotes the central wave number corresponding to central frequency $k_0 = \omega_0/c$ and φ is a constant phase factor. The result shows that the length of the interference pattern is $L = cT_0\sqrt{(1+a^2)/2}$ and the modulation of the interference pattern is described by a Gaussian function. Periodicity of the fringes at position x can be described by the corresponding wave number $k_K(x)$, which is calculated as the first derivative of the argument of the cosine function:

$$k_K(x) = 2 \left(k_0 - \frac{ax}{c^2 T_0^2 (1+a^2)} \right). \quad (11)$$

This equation shows that the wave number of the interference pattern is a linear function of x . Here we recall that the Bragg condition for reflection is fulfilled at position x when the wave number of the Bragg grating (i.e., the phase-volume hologram written by the interference pattern) is $k_K(x) = 2|k_P| = 2\omega/c$, where ω denotes the angular frequency of the electric field. Calculating the wave number of the electric field as the function of x corresponding to the chirped optical pulse at time $t = 0$, we obtain

$$k_P(x) = k_0 - \frac{2ax}{c^2 T_0^2 (1+a^2)}. \quad (12)$$

Supposing that the pulse exhibits a relatively strong linear chirp ($a \gg 1$), we obtain:

$$k_K(x) = 2 \left(k_0 - \frac{1}{a} \frac{x}{c^2 T_0^2} \right) \quad \text{and} \quad k_P(x) = k_0 - \frac{1}{2a} \frac{x}{c^2 T_0^2}. \quad (13)$$

If all the frequency components are assumed to be reflected at the position where the Bragg condition is fulfilled, (13) shows the following: the phase-volume hologram written by the interference pattern of the two counter-propagating pulses fully compensates the dispersion of the linearly chirped pulse when the chirped pulse is reflected on the corresponding phase-volume hologram.

It is worth mentioning that the same result could have been obtained without any restriction on the chirp parameter a if the Gaussian reference pulse had been replaced with an (ideal) Dirac delta pulse in (9).

Finally, let us summarize our results from Sect. 1.1. In principle, it is possible to record a 1D phase-volume hologram compensating the linear (or higher-order) chirp of any

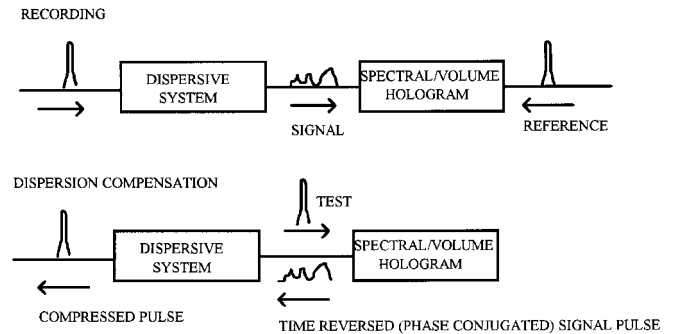


Fig. 1. Arrangement for dispersion compensation and time reversal of femtosecond pulses by means of femtosecond holography

broadband laser pulse if we are able to provide a dispersion-free reference pulse of high enough bandwidth for the recording. The structure of *the recorded phase-volume hologram preserves the dispersive features of the chirped pulse, converting its $\tau(\omega)$ function to the spatial domain*. When a chirped pulse is reflected on the corresponding phase-volume hologram, its dispersion is compensated and we obtain a practically dispersion free, i.e. transform limited, reflected pulse.

In order to obtain a time-reversed replica of the signal pulse, the signal pulse must be replaced by a dispersion-free read-out pulse, as shown in Fig. 1. The arrangement might well be suited for dispersion compensation in CPA systems, in which the temporal spread of the (i) stretched, then (ii) time-reversed, and finally (iii) amplified seed pulses can be easily (iv) compensated by using the pulse-stretching elements.

1.2 Femtosecond spectral holography

Spectral holography [37, 42] may be considered as a temporal analog of traditional spatial-domain Fourier-transform holography. In traditional holography the spatially patterned signal beam is recorded as a set of fringes as a result of interference with a spatially uniform reference beam. When illuminating the hologram with a uniform read-out beam, we reconstruct either the real or conjugate image of the original signal beam, depending on the geometry. In the time domain, the reference is (an ideal) short pulse with a broad, regular spectrum. The signal is a shaped pulse with a frequency-dependent phase and amplitude, i.e., a complex amplitude function. During holographic recording in a “2- f ” system, the complex amplitude of each spectral component of the signal pulse is recorded. When illuminating the spectral hologram, we recall either a real or a time-reversed (conjugate) copy of the signal pulse, also depending on the geometry. *One of the possible applications of spectral holography is full dispersion compensation* since the time-reversed (conjugated) signal pulse is transformed back to its original temporal (and spatial) shape when passed through the same apparatus that caused its temporal (and spatial) distortion (see Fig. 1). It is worth noting here that when we measure the dispersion of an optical element (e.g., the solid-state gain medium) using the technique termed *spectrally resolved white-light interferometry* [38], and design a chirped dielectric mirror for dispersion compensation, we practically do the same: we record the interference pattern of a signal and reference beam in the frequency domain (using a white-light source, not a mode-locked laser; see Sect. 2.4 for details), and then we retrieve the phase vs. frequency function corresponding to the medium by processing the spectrally resolved interference pattern recorded on a CCD camera. With this information, we make a coating design with the same dispersive properties that we measured over the wavelength range of interest, but with opposite sign (dispersion compensation), not forgetting the technological limitations.

In spectral holography, one of the crucial questions is how to provide a chirp-free, short reference pulse with a broad, regular spectrum for the recording. In CPA systems, a properly shaped seed pulse might well be suited for such purposes. In pulse-compression schemes developed for compression of

white-light continuum, subsequent recording of spectral holograms with narrow band reference and signal pulses with adjustable time difference between the two pulses (and adjustable exposure time) might be the solution to the problem.

Because of certain technological limitations on realizable index profiles and the overall layer thickness existing in current optical thin-film technology, we considered alternative holographic solutions for broadband dispersion control in femtosecond CPA systems and in experiments dealing with white-light-continuum compression. Furthermore, optical thin-film devices such as chirped mirrors are not capable of following the dynamic spatial and/or temporal changes in the systems mentioned above that call for subsequent readjustment of these systems to restore the optimal dispersion and thus the pulse width of such systems. One of the possible solutions of this last problem is to use dynamic (spectral) holography, i.e., using photorefractive media instead of conventional holographic media for spectral holography. Recently, some promising preliminary experiments to this end were performed by Danailov et al. [43].

1.3 Fourier-transform synthesis of chirped mirrors

Bearing in mind the analogy between phase-volume reflection holograms and chirped mirrors discussed in Sect. 1.1, let us briefly recall our previous results published in detail in [22].

Optical coating designers widely use the Fourier-transform technique for designing graded-index optical filters, often known as rugate filters, with prescribed spectral properties. These works are based on the papers of Sossi and Kard, who showed that [44–46]

$$\frac{1}{2} \int_{-\infty}^{\infty} \frac{d \ln[n(x)]}{dx} \exp(ikx) dx = Q(k) \exp[i\Phi(k)], \quad (14)$$

where $n(x)$ is the refractive index, $k = 2\pi/\lambda$ is the wave number in air, and x is twice the optical distance from the center of the inhomogeneous layer to physical position z :

$$x = 2 \int_0^z n(u) du. \quad (15)$$

In (14), $Q(k)$ is an appropriate function of the desired reflectance or transmittance. Using partial integration and a Fourier transform, one can derive

$$\ln \left[\frac{n(x)}{n_0} \right] = \frac{i}{\pi} \int_{-\infty}^{\infty} \frac{Q(k)}{k} \exp \{i[\Phi(k) - kx]\} dk, \quad (16)$$

when $n(\infty) = n(-\infty) = n_0$, and $Q(k)$ and $\Phi(k)$ are even and odd functions of k , respectively.

In general, optical coating design techniques based on (16) differ in the choice of $Q(k)$ and $\Phi(k)$ [44–52], which are usually termed Q function and phase factor, respectively. A variety of techniques exist because a simple, “universal” Q function and phase factor have not been found. However, different approximate formulae have been successfully applied in the case of a smooth refractive-index dependence. It

has been revealed that *distortions in the Fourier transformation originate from neglecting the multiple internal reflections in (14) (see [50, 51]), the effect of which is striking in the case of dielectric structures consisting of discrete layers with high refractive-index ratios (n_H/n_L)*. In Sect. 1.1, the analogy between 1D volume reflection holograms and chirped mirrors was established. In general, we can say that *by controlling the amplitudes and phases of the gratings with various spatial frequencies forming the reflection hologram, one may control the amplitude and phase of each spectral component in a diffracted optical signal*.

In the field of optical interference coatings, however, the phase factor for optical coating design has not usually been considered by designers because the phase change on reflection is rarely specified for these optical devices. Later on, it was recognized that solutions of rugate filter synthesis problems depend greatly on the choice of the phase factor [47–49, 52, 53]. Since the phase shift on reflection was found not to be uniquely connected with the amplitude reflectance modulus [52], it could be efficiently utilized to modify the refractive-index profile without affecting the spectral performance.

In [22], our goal was to find a general formula to help us in designing high-performance dielectric high reflectors for dispersion control in femtosecond lasers, i.e. mirrors with prescribed dispersion properties. Taking into account the analogy between optical coatings and reflection holograms, we chose the Q function and phase factor as the amplitude and phase of the complex amplitude reflectance, $r(k)$, respectively:

$$Q(k) = |r(k)|, \quad (17a)$$

$$\Phi(k) = \varphi_r(k), \quad (17b)$$

where $\varphi_r(k) = \arg[r(k)]$.

In spite of its approximate nature, (16) supplemented with (17a, b) were the main results of [22]. It was demonstrated that the formulae were well suited for constructing chirped dielectric rugate mirrors with preset phase and amplitude characteristics.

In a number of papers [47, 51, 52], it has been shown that if one introduces a linear phase

$$\Phi(k) = \Delta x k, \quad (18)$$

in (16) it results in a displacement Δx of the refractive-index profile along the x axis. By differentiating with respect to k , we can write (18) in the form of

$$\Delta x = d\Phi(k)/dk, \quad (19)$$

which is the *time-shifting theorem of Fourier analysis*. Previously, the theorem was successfully exploited to significantly reduce the optical thickness of synthesized rugate filters and control the shape of the refractive-index variation without affecting the spectral performance [47, 48, 53]. In [53], a general formula for the numerical calculation of the “optimal” phase function corresponding to the given design goal of reflectance versus wavelength (or wave number) function has been presented, which results in thinner rugate filters or lower index contrast than alternatives that arbitrarily constrain the phase.

We recall that the frequency dependent group delay (τ) upon reflection from a mirror is calculated in a similar manner:

$$\tau = d\varphi_r(\omega)/d\omega, \quad (20)$$

where $\varphi_r(\omega)$ is the frequency-dependent phase change on reflection, and $\omega = ck$ is the angular frequency of the incident electromagnetic wave. In order to relate (19) to (20), we calculated the increase in the group delay (τ_{DP}) upon reflection corresponding to the displacement of the refractive-index profile, e.g., a dielectric mirror, simply by dividing the increase in the optical path x by c , the speed of light in vacuum:

$$\tau_{DP} = 2\Delta x/c. \quad (21)$$

Here we would like to comment on (16) in connection with graded-index reflective structures, using some simple physical terms. First, *nonzero reflectivity at wave number k (or at wavelength $\lambda = 2\pi/k$) calls for sinusoidal modulation in the logarithmic refractive-index profile along the x axis with a periodicity $\lambda_{n(x)} = \lambda/2$, corresponding to $k_{n(x)} = 2k$* . Notice that the first term within the integral in (14), which can also be written in the form of $n'(x)/n(x)$, stands for the reflectance amplitude due to Fresnel reflection at position x inside the inhomogeneous dielectric layer. The expression describes the change in the index divided by the average index, which can be derived from the classical Fresnel formula. For higher reflectances, higher amplitude modulations, i.e. higher Fresnel reflections, are required, and *the modulation for a given value of the amplitude reflectance is inversely proportional to wave number k* . It also follows from (14) that *mirrors with broad reflectance bands and phase factors set to zero, i.e., dispersion-free mirrors, require high refractive-index modulations over very short optical distances, which leads to physically unrealizable solutions*. It is worth mentioning here that this constraint on the refractive-index modulation is analogous to the maximum intensity limit in pulsed laser amplifier systems for avoiding nonlinear effects such as self-focusing. The former problem can be solved by spatially “chirping” the frequency components of the mirrors (chirped mirrors), while the latter one can be efficiently eliminated by temporally “chirping” the frequency components of the pulse (CPA, or chirped pulse amplification systems). Note, however, that using dielectric mirrors at oblique angles of incidence for s-polarized light, one can increase the effective refractive-index modulation and thus the reflectivity band of standard dielectric $\lambda/4$ or chirped mirrors (see Sect. 2.5.2).

In the following, we present as an example a chirped dielectric mirror design, the structure of which is derived from (16). Dispersive and spectral properties of the design are calculated with the classic scattering matrix multiplication technique [12, 13] and compared to their prescribed values.

We define a second order phase factor, $\Phi(k)$ as the function wave number, i.e. a second-order phase shift on reflection [see (17b)] written in the following form:

$$\Phi(k) = d_0 + d_1(k - k_0) + d_2(k - k_0)^2. \quad (22a)$$

Furthermore, we define the Q function $Q(k)$, i.e. the modulus of the complex amplitude reflectance [see (17a)], as a Gaus-

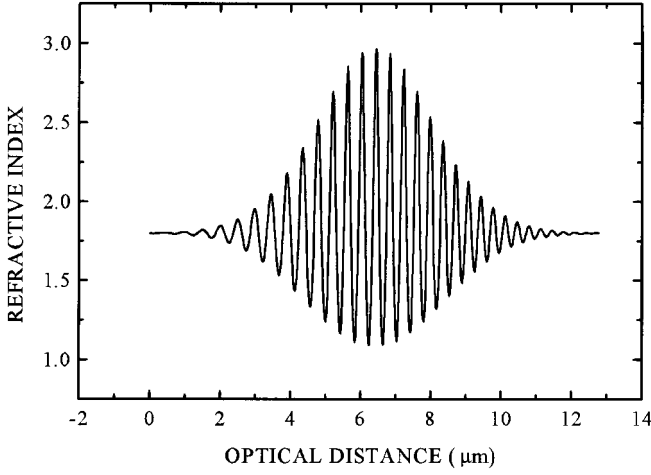


Fig. 2. Refractive index profile of a chirped graded-index dielectric mirror design constructed by the use of Fourier transform [22]

sian function:

$$Q(k) = \exp \left[-\frac{(k - k_0)^2}{2\sigma^2} \right]. \quad (22b)$$

Calculating the frequency-dependent displacement $\Delta x(k)$ of the refractive profile along the x axis using (19), one obtains:

$$\Delta x(k) = d_1 + 2d_2(k - k_0), \quad (23)$$

or equivalently, using (21):

$$\tau_{DP}(k) = 2 \frac{d_1 + 2d_2(k - k_0)}{c}, \quad (24)$$

which is a linear function of the wave number, thus the angular frequency of the incident electromagnetic field.

Equation (23) shows that the different spatial frequency components are shifted linearly along the x axis as a function of k , i.e. the second-order phase term in (22a) results in a chirped dielectric rugate structure, as shown in Fig. 2. The parameters that we used during its computations with

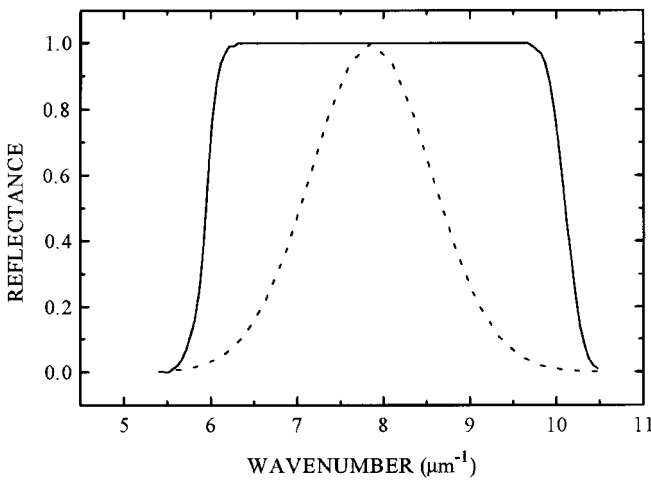


Fig. 3. Specified (dashed) and computed (continuous line) reflectance of chirped graded-index mirror shown in Fig. 2

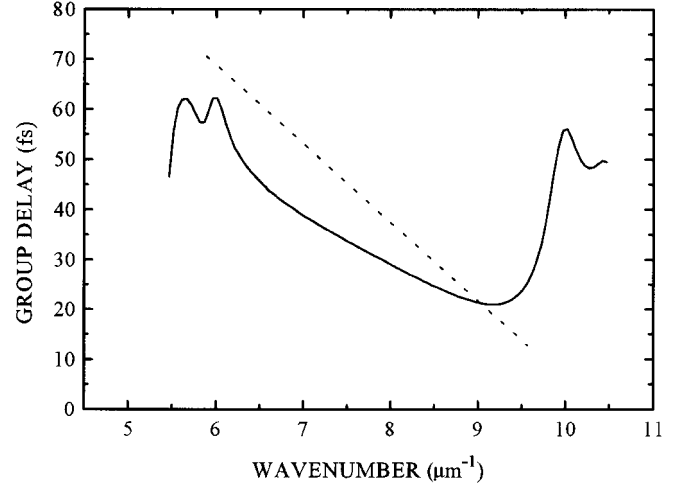


Fig. 4. Specified (dashed) and computed (continuous line) group delay of chirped graded-index mirror shown in Fig. 2

(16) were: $k_0 = 2\pi/0.4 \mu\text{m}^{-1}$, which corresponds to our selected mirror central wavelength of $0.8 \mu\text{m}$; $\sigma = 1.4 \mu\text{m}^{-1}$; $d_1 = 0 \text{ rad}$; $d_2 = 0 \mu\text{m}$; $d_3 = -0.589 \mu\text{m}^2$. The refractive index of the surrounding medium has been set to $n_0 = 1.8$. To obtain high enough reflectances, we multiplied the right-hand side of (16) by a factor of 8. With the method published by Southwell [54, 55], the refractive-index profile shown in Fig. 2 can be converted to a two-index solution by taking into account dispersion of the coating materials as well. The two-valued refractive-index profile obtained after the conversion can be used as an initial design for further refinement, which will be discussed later in detail.

In Fig. 3, the computed reflectance of the chirped structure is presented along with the prescribed reflectance values. It is worth noting that the structure exhibits practically 100% reflectance from wave numbers of $6.35 \mu\text{m}^{-1}$ to $9.35 \mu\text{m}^{-1}$, which correspond to wavelengths of $0.989 \mu\text{m}$ to $0.671 \mu\text{m}$, respectively. Calculating the group delay introduced by the chirped mirror by using (20), the result of which is shown in Fig. 4, we have found that the group delay decreases monotonously with frequency (or wave number) over most of the high reflectivity band of the mirror. The mirror exhibits nearly constant GDD over the $6.5\text{--}9 \mu\text{m}^{-1}$ wave number range corresponding to the wavelength range from 1.0 to $0.7 \mu\text{m}$. We note that a constant group delay of $\tau_0 = 2 \times 6.388 \mu\text{m}/(0.3 \times 10^{-9} \text{ m/s}) = 42.583 \text{ fs}$ has been added to the prescribed group-delay values. The calculated group delay vs. wave number function of the chirped structure slightly differs from the specified linear function; however, the design can be utilized as a starting design for further refinement after the conversion method mentioned above has been used.

2 Design of chirped mirrors consisting of discrete layers

In this section, first we describe how to obtain an initial design consisting of discrete layers from the formulae presented in Sect. 1.3: viz. we summarize the conversion methods presented in [54, 55]. Then we assume that we have an initial design either obtained by the use of Fourier transformation and the conversion procedure or by using other designs pre-

sented elsewhere for further optimization [21, 28, 56]. Our aim is to find the best solution for a certain application problem, bearing in mind the constraints on the parameters set by the technology (e.g., the refractive indices of available coating materials, the upper and lower limits on the thickness of the individual layers, the maximum overall thickness of optical coating), all of them depending on the technology utilized for coating deposition. Not losing the generality, we restrict our treatment to the simplest practical case, in which the (chirped) laser mirrors are built of alternate discrete layers of a high-index (TiO_2) and a low-index (SiO_2) materials.

2.1 Conversion of graded-index chirped mirror structures to discrete layer realizations

We thought that it might be interesting to present the chronological development of chirped mirrors leading to the first designs consisting of nearly quarterwave layers of TiO_2 and SiO_2 [21, 56]. First, we investigated the dispersive properties of dielectric structures derived from the formulae in Sect. 1.3, and described by the following equation:

$$n(x) = \sqrt{n_H n_L} \exp \left\{ \ln \sqrt{\frac{n_H}{n_L}} \exp \left(-\frac{x^2}{2\sigma^2} \right) \times \sin[x(k_0 + c_1 k_0 x)] \right\}. \quad (25)$$

In (25), n_H and n_L denote the maximum and minimum values of the refractive-index profile function such that $n(x)_{\text{MAX}} = n_H = 2.3$ and $n(x)_{\text{MIN}} = n_L = 1.45$, according to the actual upper and lower limits of the refractive indices available; x is defined as the optical distance similar to (15) (without the multiplication factor 2); σ denotes the width of the Gaussian envelope function; k_0 denotes the wave number corresponding to our selected central wavelength (λ_0) fulfilling the Bragg condition $k_0 = 2k$, where $k = 2\pi/\lambda$, and c_1 is a linear (spatial) chirp parameter. With the parameters $\sigma = 2^{1/2}$ and $c_1 = \pm 0.02$, we obtained increasing or decreasing group-delay functions with the frequency depending on the sign of

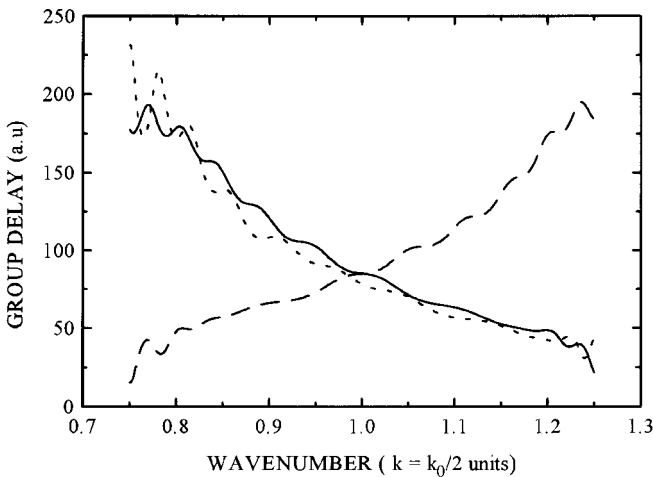


Fig. 5. Computed group delay vs. wavelength functions of positively (dashed) and negatively chirped (continuous line) graded-index profiles described in the text. The dotted curve corresponds to the discrete valued index profile shown in Fig. 6

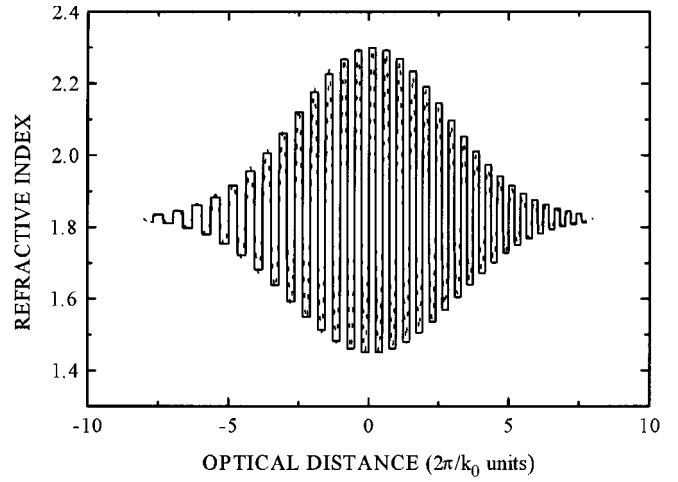


Fig. 6. Refractive index profile of a discrete valued chirped dielectric mirror obtained by replacing the $\sin(kx)$ function with a $\text{sign}[\sin(kx)]$ function in (25)

the spatial chirp parameter c_1 as shown in Fig. 5. We assumed the refractive indices on both sides of the dielectric structure be equal to $n_{\text{ave}} = (n_H n_L)^{1/2}$. The group delay functions were calculated by using the scattering matrix method [12, 13] after dividing the structure into 2048 sub-layers, which were assumed to have uniform refractive indices. As can be seen in the figure, the group-delay functions exhibit a positive or negative slope vs. wave number (frequency), depending on the sign of the spatial chirp. However, with some superimposed oscillatory behavior. We found that the amplitude of this oscillatory behavior is connected with parameters such as the shape and width (σ) of the envelope function, the chirp parameter (c_1) and the amplitude of the refractive-index modulation. It is worth mentioning here that a similar effect was observed by Southwell [57] in the case of (non-dispersive) rugate filters as well, in which the oscillation was considerably reduced by a proper choice of the apodization function. It fits well with our previous theoretical calculations: when super-Gaussian or rectangular apodization functions were used, the oscillatory behavior was found to be even more pronounced. It will be shown later that the same behavior of the dispersive properties was observed in the case of chirped dielectric mirrors consisting of discrete layers.

Next we investigated similar structures consisting of nearly quarterwave-thick layers with appropriately chosen refractive indices similar to that shown in Fig. 6, i.e., the $\sin(x)$ function in (25) was replaced by a $\text{sign}[\sin(x)]$ function and the refractive-index modulation was kept constant within a nearly quarterwave layer. The corresponding group delay vs. wave number function is plotted in Fig. 5 with dots. This gives practically the same curve obtained for the continuously varying refractive-index profile determined by (25) with similar construction parameters. The group delay is computed for beam propagation to the direction of negative optical distances.

It must be pointed out that by reversing the order of the deposition of the layer sequence (or the direction of the incoming beam), we reverse the slope of the group delay vs. wave number (frequency) function of the chirped dielectric mirror structure, and the following condition is approximately

fulfilled:

$$\tau_R \Big|_{k_0 - \Delta k} \approx \tau \Big|_{k_0 + \Delta k}, \quad (26)$$

where τ_R denotes the group delay vs. wave number function of the *spatially mirrored structure*. In practice, it means that *an initial chirped mirror design exhibiting a negative GDD can be easily converted to another design exhibiting a positive GDD of the same absolute value by revising the layer sequence, even in the case of chirped mirrors exhibiting a two-valued refractive-index profile*. In principle, for example, it would be possible to stretch and compress a bandwidth-limited laser pulse to its original shape by properly designed chirped mirrors when the pulse first hits the structure from the right-hand side (for stretching) and then from the left-hand side (for compression). This feature directly follows from (16) and (19) previously presented in [22]. Subsequently, similar ‘‘bulk chirped Bragg reflectors’’ for light-pulse compression and expansion were proposed by Tournois and Hartemann [58].

Let us mention here that if we assume we do not have a lower limit to the layer thickness, the refractive-index profile shown in Fig. 6 can be directly converted to a solution consisting of alternate layers of high- and low-index coating materials (such as TiO_2 and SiO_2) exclusively with the use of the first conversion formula presented below. The formula shows that when two-layer materials with small enough optical thickness (e.g., 0.1 in $\lambda/4$ units) relative to the operation wavelength (λ) are mixed, the composite layer exhibits an effective refractive index between the refractive indices of the two pure layer material, depending on their physical thickness ratio. In (27), n_i is the refractive index of the i th (nearly quarterwave) layer and d_H and d_L denote the physical layer thicknesses of the elementary sublayers [54]:

$$n_i^2 = \frac{n_H^2 d_H + n_L^2 d_L}{d_H + d_L}. \quad (27)$$

Practical realization of such structures depends on the accuracy in the thickness measurement of the coating deposition technology applied.

In general, we prefer optical coating designs consisting of nearly quarterwave layers for technological purposes (e.g., minimizing stress in the coating, thickness control accuracy). Using the results published in [54, 55], it is possible to convert structures consisting of N layers of different refractive indices (such as shown in Fig. 6) into a two-index solution consisting of $2N$ layers: we must convert all layers into HL (or LH) equivalents by using the following equations for the physical layer thicknesses $d_{i,H}$ and $d_{i,L}$

$$d_{i,H} = \frac{n_i^2 - n_L^2}{n_H^2 - n_L^2} d_i, \quad (28a)$$

$$d_{i,L} = d_i - d_{i,H}, \quad (28b)$$

Alternative methods of constructing two-index realization may also be based on the recent work of Tournois [58]. It is worth pointing out that in [58], two basic solutions were proposed: (i) chirped Bragg reflectors consisting of halfwave stacks (i.e., halfwave chirped mirrors), and (ii) chirped Bragg

reflectors consisting of quarterwave stacks (i.e., quarterwave chirped mirrors). In the former case, thin layers of thickness $t_i \ll \lambda$ are immersed in a medium of a different refractive index. The thickness t_i of the i th layers permits one to adjust the modulus of the elementary reflection coefficient r_i in accordance with the formula presented in Ref. [58]. The stack is called halfwave because the optical distance between two adjacent thin layers is $\lambda/2$. However, when thin-film deposition technology is concerned, the halfwave stack solution causes serious technological problems, such as mentioned above: the relatively small thickness of the low refractive index layers compared to the high index components considerably increases the *internal stress* of the coating; stress of this nature easily destroys a coating consisting of a large number of layers. In addition to the standard (nearly quarterwave stack) chirped dielectric mirrors with which we usually work, a combination of quarterwave layers and the thin layers mentioned above has been proposed in [58].

In order to show the powerfulness and the weakness of the Fourier-transform technique and the conversion routine described above, we present a chirped mirror design developed for full dispersion compensation in the white-light continuum compression experiment described in [35]. Briefly, the estimated group delay dispersion of the white-light continuum is $\cong 380 \text{ fs}^2$ at 600 nm and decreases to $\cong 220 \text{ fs}^2$ at 1 μm [35]. In order to compensate the nonlinear chirp of the continuum, chirped dielectric mirrors exhibiting high reflectivity and negative GDD with superimposed negative TOD from 600 nm to 1200 nm were developed with the design method described above. We introduced a quadratic spatial chirp parameter c_2 to (25), and modified the envelope function in order to obtain index modulation best fitting the conversion routine parameters:

$$n(x) = \sqrt{n_H n_L} \exp \left\{ a \frac{k_0}{k} \ln \sqrt{\frac{n_H}{n_L}} \exp \left(-\frac{x^4}{2\sigma^4} \right) \right. \\ \left. \times \sin [x(k_0 + c_1 k_0 x + c_2 k_0 x^2)] \right\}, \quad (29)$$

where $n(x)_{\text{MAX}} = n_H = 2.315$ and $n(x)_{\text{MIN}} = n_L = 1.45$, $k_0 = 2 \times 2\pi/0.8 \mu\text{m}^{-1}$ corresponding to our selected central wavelength of 800 nm, $\sigma = 5.49 \mu\text{m}$, $c_1 = 0.05$ and $c_2 = -0.002$ are dimensionless linear and quadratic spatial chirp parameters, $a = 1.35$ is a dimensionless amplitude modulation factor. In Fig. 7, the refractive-index profile obtained from (29) is shown. First, the graded-index structure was converted to a step-index equivalent whose refractive-index profile is shown in Fig. 8. Second, the step-index profile was converted to a two-index equivalent (Fig. 9) by using (28a, b). It is worth mentioning here that the conversion routine results in a very interesting structure: the highest index modulations in the step-like index profile are converted to a $\lambda/4$ stack of high- and low-index materials, whereas the lowest modulations are converted to $\lambda/8$ stacks exhibiting practically zero reflectivity at wavelength λ , as shown in Fig. 9. Between these two extremes, the optical thickness of the alternating high- and low-index layers gradually changes, resulting in a smoothly varying coupling coefficient over the layer structure. Note that partial reflectances at layer interfaces of a $\lambda/4$ stack meet in phase, resulting in a high overall reflectivity, whereas in a $\lambda/8$ stack they meet in anti-phase resulting in a low overall reflectivity. Computed group-delay functions

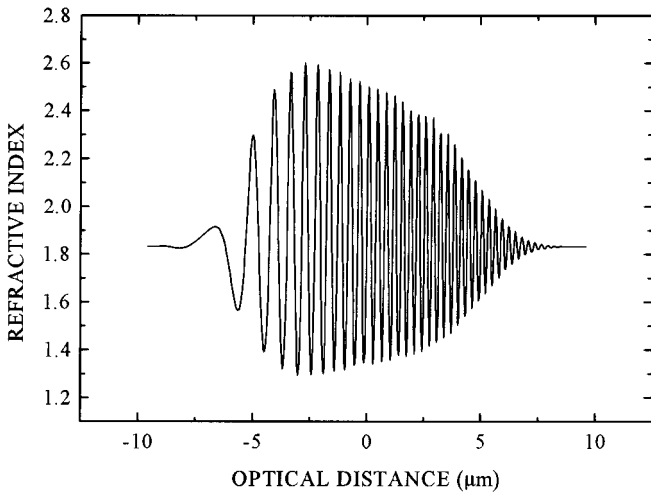


Fig. 7. Refractive index profile of an ultra-broadband gradient chirped dielectric mirror corresponding to (29). The mirror was developed for full dispersion compensation in the white-light continuum compression experiment described in [35]

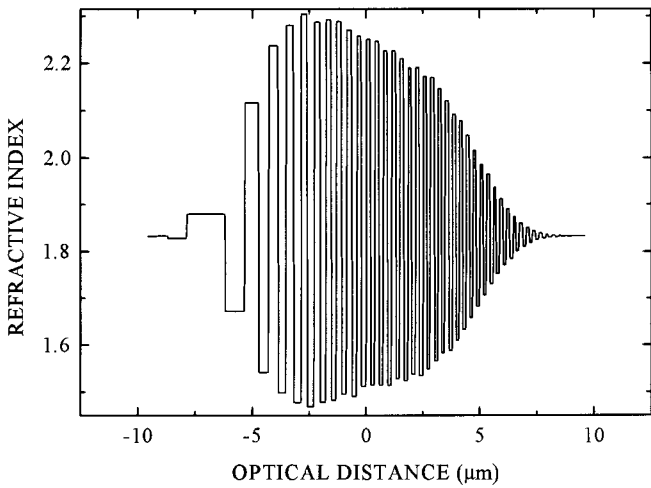


Fig. 8. Refractive index profile of the step-index equivalent of the graded-index profile shown in Fig. 7

and reflectance vs. wavelength functions of the graded-index structure, the step-index structure, and the two-index equivalent are plotted in Figs. 10 and 11. As one would expect, the graded-index structures exhibit nearly ideal reflectance and group delay functions and the step-index equivalent still shows a very similar spectral response, in spite of the high partial reflectances at the layer interfaces. The two-index equivalent, however, is far from being an ideal solution to our application problem because of some resonant features occurring in both the reflectance and the group-delay spectrum. Additionally, the structure still requires impedance-matching layers at the substrate-coating and air-coating interfaces. After a computer optimization process, described in Sect. 2.2, however, it was possible to eliminate the resonant structures in both the reflectance and group delay functions (see Figs. 12 and 13). Oscillations in the group-delay function has been efficiently reduced by depositing two similar chirped mirror designs with slightly shifted central wavelengths and using them in pairs (see Fig. 13). As a preliminary experimental re-

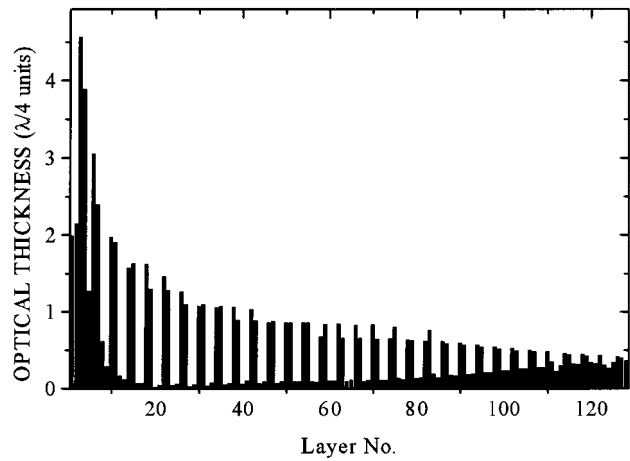


Fig. 9. Optical thickness coefficients of the two-index HL equivalent layers corresponding to the step-index profile shown in Fig. 8. Note that the highest amplitude index modulations are converted basically to $\lambda/4$ stacks while the lowest index modulations correspond to $\lambda/8$ stacks

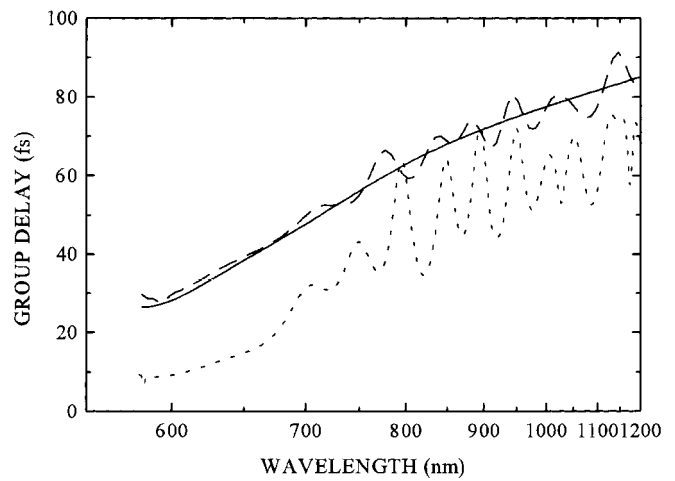


Fig. 10. Computed group delay vs. wavelength functions of the index profiles shown in Fig. 7 (continuous line), Fig. 8 (dashed line) and Fig. 9 (dotted line)

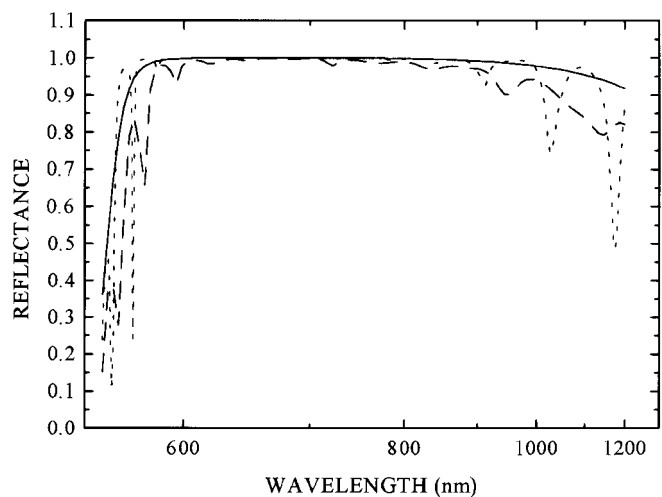


Fig. 11. Computed reflectance vs. wavelength functions of the index profiles shown in Fig. 7 (continuous line), Fig. 8 (dashed line) and Fig. 9 (dotted line)

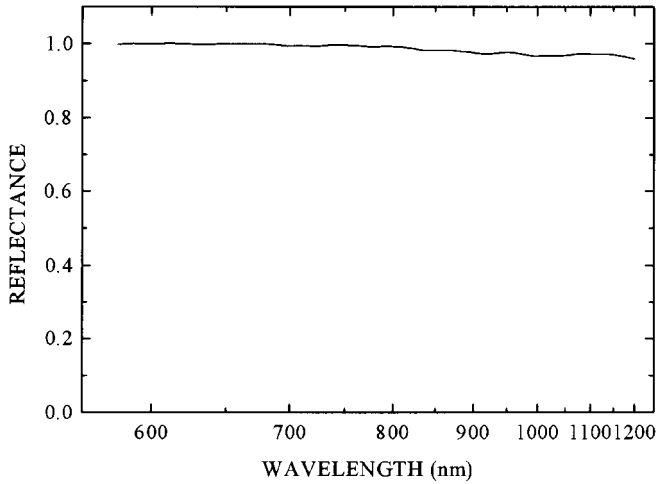


Fig. 12. Computed reflectance vs. wavelength function of the two-index equivalent after adding impedance matching layers at the substrate/coating and coating/air interfaces and after computer optimization

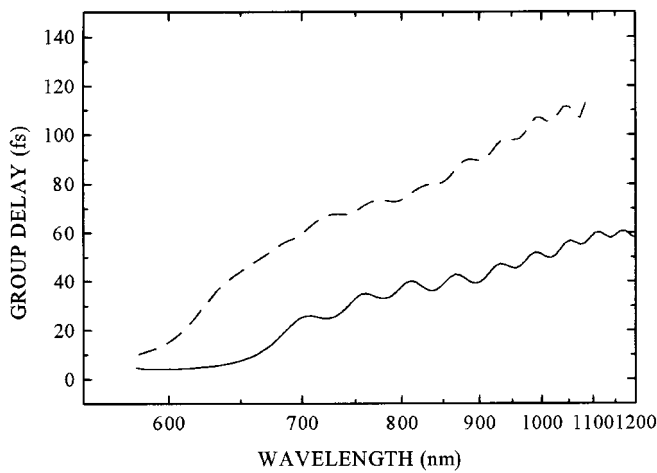


Fig. 13. Computed group delay vs. wavelength function (*continuous line*) of the two-index equivalent after adding impedance matching layers at the substrate/coating and coating/air interfaces and after computer refinement. Combination of two such chirped mirrors with slightly shifted central wavelengths results in lower oscillation in the overall group delay function (*see dashed line*)

sult, 6-fs pulses were obtained in the experiment described in [35] with the exclusive use of 4 pieces of dispersive mirrors. A typical measured autocorrelation trace is shown in Fig. 14.

2.2 Computer optimization of the design

There is a practical problem in connection with the Fourier-transform technique described above: the dielectric layers are deposited on a substrate, e.g., on BK7 glass ($n_S \cong 1.51$) or fused silica ($n_S \cong 1.45$), whose refractive indices do not fit the average value of the two coating materials used for evaporation. By way of contrast, the situation is even worse on the opposite side: the refractive index of air is 1.0. In the case of graded-index (e.g., chirped graded-index) structures, the problem can be efficiently diminished by the use of quintic matching layers, which is described in [59]. In

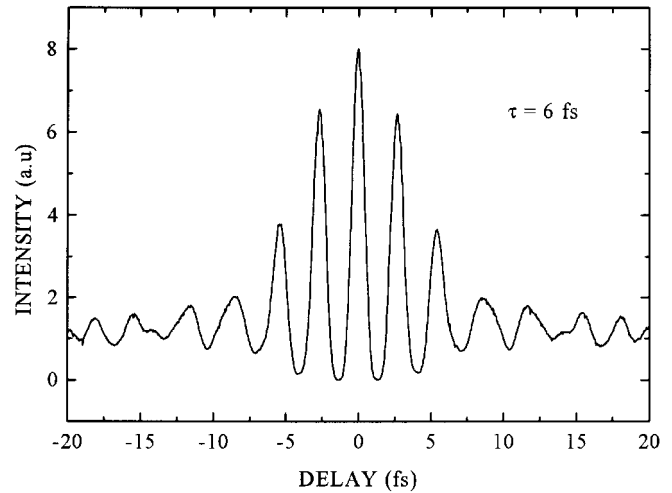


Fig. 14. Measured interferometric autocorrelation trace of a white-light continuum being compressed merely by 4 pieces of ultra-broadband dispersive chirped mirrors (see the experiment described in [35])

the case of chirped mirror structures consisting of nearly quarterwave layers, however, it was difficult to find an exact analytical solution to the problem. Practically, it is an impedance-matching problem that we usually face when designing AR coatings or dichroic mirrors that are transparent for the pump wavelengths. A straightforward way of solving the problem is properly choosing the optical thickness of a limited number of top and bottom (impedance-matching) layers of the design. In practice, *numerical optimization procedures were used* in order to obtain suitable solutions of different application problems.

Numerical procedures are widely used for optical coating design. For a review on these, see the paper by Dobrowolsky and Kemp [60]. Most of the optimized coating designs are obtained by using the so-called simplex method [60]; however, for the *initial global search*, slower but more efficient algorithms such as *generalized simulated annealing* [61, 62] or the *genetic algorithm* (GA) [63] are proposed. Nevertheless, the efficiency of each of the methods mentioned above strongly depends on the *proper choice of the target function and the performance (or merit) function*. Additionally, one has to *properly define the parameter space where the best solution of a specific application problem must be found* in accordance with the technology to be used for the coating deposition. In the following, this parameter space is called the *search space*. In general, it is a $2N$ -dimensional space, where N is the number of layers in the system to be synthesized. One solution of the problem (a coating design) is described as a $2N$ -dimensional vector $\mathbf{X} = \{(t_1, n_1), (t_2, n_2), \dots, (t_N, n_N)\}$, where t_i and n_i represent the thickness and the refractive index of the i th layer of the system, respectively. To obtain realistic solutions, the refractive indices and the thickness must satisfy the following constraints: $n_L < n_i < n_H$, and $0 < t_i < t_{MAX}$ for each i value, where n_H and n_L correspond to the highest and lowest refractive indices available. Without going into detail and referring to some previous work [21, 56], we define below two general *performance functions* for the amplitude and the phase properties, which are denoted as M_R , and M_{GDD} , respectively. In practice, we have always had to find a compromise

between the tolerances corresponding to the amplitude (δR) and the dispersive (δD_{GDD}) properties, whose overall value must be minimized by any of the optimization methods mentioned above. The performance functions are defined by the following equations:

$$M_{\text{R}}(\mathbf{X}) = \frac{1}{p} \sum_{j=1}^p \{ [R(\lambda_j) - R_{\text{OPT}}(\lambda_j)] / \delta R_j \}^2, \quad (30)$$

$$M_{\text{GDD}}(\mathbf{X}) = \frac{1}{p} \sum_{j=1}^p \{ [D_{\text{GDD}}(\lambda_j) - D_{\text{GDD,OPT}}(\lambda_j)] / \delta D_{\text{GDD},j} \}^2, \quad (31)$$

where $R(\lambda_j)$ and $R_{\text{OPT}}(\lambda_j)$ are the calculated and desired reflection values, respectively, of the actual layer structure (fully described by vector \mathbf{X}) at wavelength λ_j . Similarly, $D_{\text{GDD}}(\lambda_j)$ and $D_{\text{GDD,OPT}}(\lambda_j)$ are the calculated and desired group-delay dispersion ($D_{\text{GDD}} = \delta^2 \varphi / \delta \omega^2$) values at wavelength λ_j . Here $\varphi(\omega)$ denotes the phase change upon reflection from a dielectric mirror at frequency ω . For oblique angles of incidences, $R(\lambda_j)$, $R_{\text{OPT}}(\lambda_j)$, $D_{\text{GDD}}(\lambda_j)$ and $D_{\text{GDD,OPT}}(\lambda_j)$ should correspond to the actual and desired reflectivities and the calculated and desired group-delay dispersion functions for s- or p-polarized light, respectively. *The novelty of our construction method is in the use of the merit function defined by (31); to the best of our knowledge, this has never been used before the publication of [21, 56] for optical coating designs.* Let us comment on why the GDD vs. frequency (or wavelength function) is usually preferred compared to the phase vs. frequency [$\varphi(\omega)$] or group delay ($\tau = \partial \varphi / \partial \omega$) vs. frequency functions. Operation of a femtosecond laser depends on the intracavity GDD rather than the round-trip time in the cavity, as discussed in Sect. 1. Upon reflection of the laser light from a (chirped) mirror, a constant group delay changes the round-trip time by only a few femtoseconds, which is very small compared to the whole round-trip time of a (usually 1-m to 2-m long) linear or ring cavity. Fixing the desired value of the group delay at a certain wavelength, we restrict the number of possible solutions, if they exist at all. However, using additional performance functions corresponding to higher-order derivatives of the $\varphi(\omega)$ function, such as the third-order dispersion ($\text{TOD} = \partial^3 \varphi / \partial \omega^3$), could be advantageous in some specific cases.

2.3 A numerical example

As an example [21, 56], let us take one of our first designs, which were obtained by optimizing the layer thickness of an initial, spatially chirped and randomized mirror structure consisting of 42 alternate discrete layers of TiO_2 and SiO_2 with optical thickness around $\lambda/4$. In this particular case, we worked with 42 D vectors only, since the refractive-index values of the individual layers were not changed during the optimization process. The refractive-index profile of the structure is shown in Fig. 15. It was obtained after several optimization processes with different target functions according to the dispersive properties of previous solutions. The corresponding optical layer thicknesses are given in the figure caption and

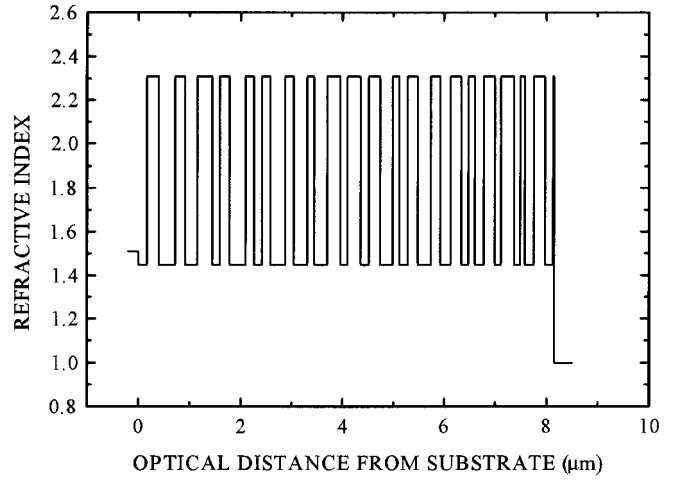


Fig. 15. Two valued refractive-index profile of a chirped dielectric laser mirror designed for full dispersion compensation in a mode-locked Ti:sapphire laser. Optical thickness coefficients of the design are [56]: S | 0.87L 1.14H 1.58L 0.98H 1.18L 1.45H 0.75L 0.96H 1.57L 0.85H 0.73L 0.84H 1.45L 0.85H 1.31L 0.69H 1.30L 1.29H 0.69L 1.30H 0.81L 1.07H 1.25L 0.67H 0.81L 0.96H 1.35L 0.88H 1.03L 1.09H 0.62L 0.66H 0.87L 1.12H 0.62L 1.21H 0.63L 0.43H 0.93L 1.07H 0.78L 0.16H | A. S: substrate, $n_{\text{S}} = 1.51$; A: air, $n_{\text{A}} = 1.0$; H and L: quarterwave layers of TiO_2 and SiO_2 , respectively, at $\lambda = 790$ nm, $n_{\text{H}} = 2.315$, $n_{\text{L}} = 1.45$

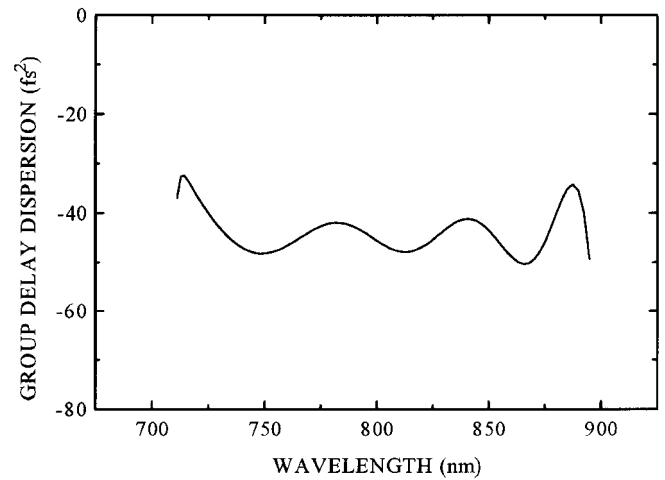


Fig. 16. Computed group delay dispersion of the chirped mirror design shown in Fig. 15

in [56]. The design was developed for full dispersion control in a femtosecond pulse Ti:sapphire laser [64]. Enhanced versions of the chirped mirror design shown in Fig. 15 were used in the experiments described, for example, in [23, 35, 64, 65]. The mirror exhibits high reflectivity and a nearly constant negative GDD of -41 ± 5 fs² over a wavelength range from 720 nm to 890 nm; the computed GDD of the design is shown in Fig. 16. The structure still shows the increasing multilayer period toward the substrate, hence we call it a chirped mirror, even though the variation is far from what we can consider regular spatial chirp.

If the electric-field distribution inside this chirped mirror is computed as a function of the wavelength, as shown in Fig. 17a, it can be seen that the penetration depth (and thus the group delay) increases approximately linearly with the wave-

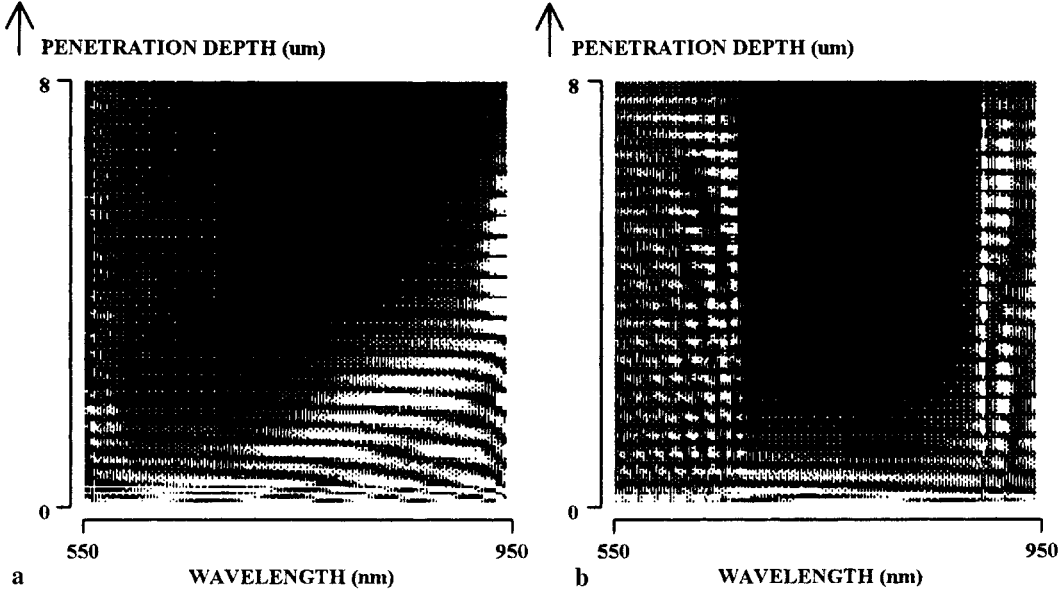


Fig. 17a,b. Computed electric-field distribution as a function of wavelength in (a) the chirped dielectric structure shown in Fig. 7 and in (b) a 44-layer low dispersion dielectric mirror consisting of alternating quarterwave layers of TiO₂ and SiO₂

length over the 720-nm to 890-nm range. For the electric-field calculations, the results presented in [66] were used. The figure also gives clear evidence of the high reflectivity of the mirror, as indicated by the disappearance of the optical field at the substrate-coating interface (penetration depth 8). For comparative purposes, the electric-field distribution inside a traditional, low-dispersion dielectric mirror consisting of 44 alternate quarterwave layers of TiO₂ and SiO₂ and centered at 770 nm is depicted in Fig. 17b. The penetration depth and thus the group delay is smallest at the central wavelength of the quarterwave mirror and symmetrically increases with the detuning. This behavior results in quarterwave mirrors having a positive third-order dispersion (TOD) [14]. It is clear that if one compares the electric-field distributions corresponding to the chirped mirror and the quarterwave mirror, chirped multilayer coatings have the potential for extending the bandwidth of standard low-dispersion quarterwave mirrors. *We note here that ultra-broadband chirped dielectric laser mirrors “must” have a certain positive TOD as well because of the same physical reason. This is why the useful range of the design presented in Sect. 2.1 is narrower than its high reflectivity range* (see Figs. 12 and 13).

The maximum achievable negative GDD of chirped mirrors is limited by the maximum group-delay difference that can be obtained between the extremes of the reflectivity range. This in turn relates to the optical thickness of the coating. A simple approximate expression for the maximum achievable group-delay difference was presented in [21]:

$$\Delta\tau_{\max} = \frac{2(t_{\text{chirped}} - t_{\text{qw}})}{c}, \quad (32)$$

where t_{chirped} is the optical thickness of the chirped mirror and t_{qw} is that of a standard quarterwave high reflector ($R > 99.5\%$) consisting of the same pair of alternating layer materials. In simplified physical terms: the required high reflectivity of the dispersive mirror calls for a minimum optical thickness of t_{qw} , and only excess layers can introduce an appreciable frequency-dependent group delay around the center of the high-reflectivity band. If we assume the group delay

to vary approximately linearly with frequency over the high-reflectivity range, the corresponding upper estimate for the GDD is simply given by the ratio of $\Delta\tau_{\max}$ to the mirror bandwidth $\Delta\omega$. For the specific case of TiO₂–SiO₂ mirrors centered around 0.8 μm , we have approximately $t_{\text{qw}} = 4 \mu\text{m}$ (21 quarterwave layers) yielding approx. $\Delta\tau_{\max} = 27 \text{ fs}$ for our 8- μm -thick structures, which is in reasonable agreement with the results presented in [21]. With the number of layers fixed, $\Delta\tau_{\max}$ scales linearly with the chosen central wavelength of the dispersive mirror. For a selected operating wavelength, $\Delta\tau_{\max}$ and thus the magnitude of broadband negative GDD can be increased only by increasing the number of layers, this number being limited by scattering and absorption losses due to structural defects and impurities in the deposited layers, respectively [14].

2.4 The effect of deposition errors

In this section, we assume that we ended up with a design consisting of alternate discrete layers of high-index (H) and low-index (L) materials after the optimization process. Before deposition of such a structure, the following questions arise. Can the design tolerate the inaccuracies in the layer thickness (and the refractive indices) appearing during the deposition process? If the answer is no, can we make a better design exhibiting lower sensitivity for deposition errors? Alternatively, can we improve the control of thickness/refractive index in our evaporation plant? In order to demonstrate the importance of these questions, we analyse the chirped mirror structure shown in Fig. 15. We calculated the average deviation of GDD from its theoretical value when each layer thickness was varied by $\pm 1\%$ of the corresponding quarterwave layer: $\Delta t_i = \pm 0.0025 \lambda_0 / n_i$. In our example, the reference wavelength is $\lambda_0 = 775 \text{ nm}$ and the refractive indices of TiO₂ and SiO₂ are $n_H = 2.315$ and $n_L = 1.45$, respectively. Dispersion data were calculated for the wavelength range of 720 to 890 nm. The result is shown in Fig. 18. The striking feature of the plot is that dispersion of *the design is extremely sensitive to deposition errors*: for some layers the deviation

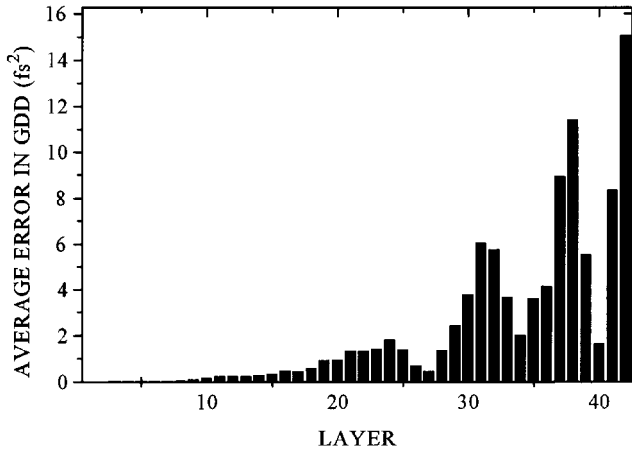


Fig. 18. The effect of deposition errors on the GDD vs. wavelength function of the chirped mirror design shown in Fig. 15

from the prescribed dispersion value is, on average, as high as 15 fs^2 , which is approximately 30% of the prescribed value. It is mentioned that the estimated variation of the layer thicknesses is a realistic value in our model; this estimated value can be applied for most evaporation plants. We do not need to mention that we were extremely fortunate with the dispersive properties of the chirped mirrors used for our first experiments; see [21, 64]. How can one improve the situation? The answer is, first, by a better design that exhibits a lower sensitivity to the deposition errors. Here we refer to the recent work by Greiner [67], who developed *robust optical thin film designs that are insensitive to the variation of layer parameters* by applying different search strategies. The design methods described in [67] can be adapted to our application problem as well. Second, the situation can be improved by applying enhanced thickness control during the evaporation. *The final solution to the problem, however, is based on the development of highly accurate methods for dispersion measurement on laser mirrors* [38, 39]. In the following, we briefly introduce our dispersion measurement apparatus and

present representative GDD data corresponding to elements of a mirror-dispersion-controlled (MDC) Ti:S oscillator [68].

Generally, the apparatus we use is a Michelson interferometer [38] illuminated by a white-light source (tungsten halogen lamp). We place a low-dispersion gold mirror in the “reference” arm and the chirped dielectric mirror to be measured in the “sample” arm. When one of the mirrors is tilted around a horizontal axis and the other mirror is vertical, horizontal interference fringes are generated by each spectral component of the white-light source at the exit plane of the interferometer. A transmission grating and an achromatic lens are used to create the spectrally dispersed image of a vertical section of the superimposed “white-light” interference fringes on a CCD array; the section is created by a vertical slit. The interference patterns corresponding to different wavelengths are linearly dispersed in the horizontal direction, as shown in Fig. 19.

In the case of Fig. 19a, a pair of *chirped mirrors developed for full dispersion control in a mode-locked Ti:S oscillator* [21, 23, 56, 64, 68] were placed in the “sample” arm of the interferometer. To record the image shown in Fig. 19b, however, a pair of chirped mirrors developed for a *prism pair chirped mirror compressor* [25, 33, 38] exhibiting *negative GDD with a superimposed positive TOD* was used.

The period of the interference fringes in the vertical direction is proportional to the wavelength when ideal flat mirrors are used for the measurement. If the mirror in the sample arm were to have no phase dispersion, the vertical pixel positions corresponding to the same phase difference, e.g., minima and maxima, would be a linear function of the wavelength [38]. Because of the second-order phase shift of one sample mirror (a) and the second-order phase shift with superimposed positive third-order dispersion of the other mirror (b) we were able to record the images shown in Fig. 19.

By storing and computer-processing the spectrally resolved interference pattern detected on the CCD, we can easily obtain the group delay and GDD versus wavelength functions of the sample mirrors within a few minutes by using a personal computer.

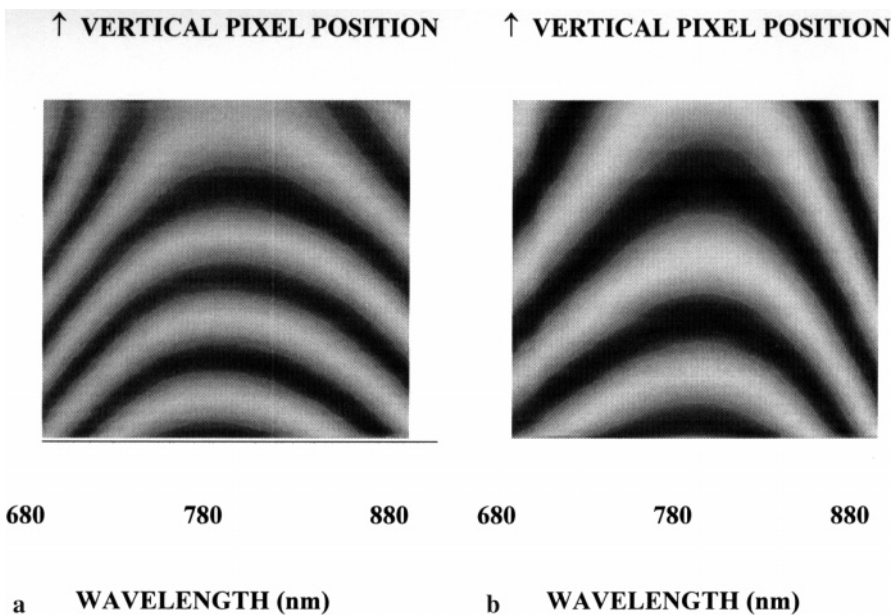


Fig. 19a,b. Spectrally resolved white-light interference fringes recorded on a CCD, when pairs of (a) chirped mirrors with a pure negative quadratic phase and (b) chirped mirrors with negative GDD and superimposed positive TOD are placed in one arm of a Michelson interferometer illuminated by a tungsten halogen lamp [38]

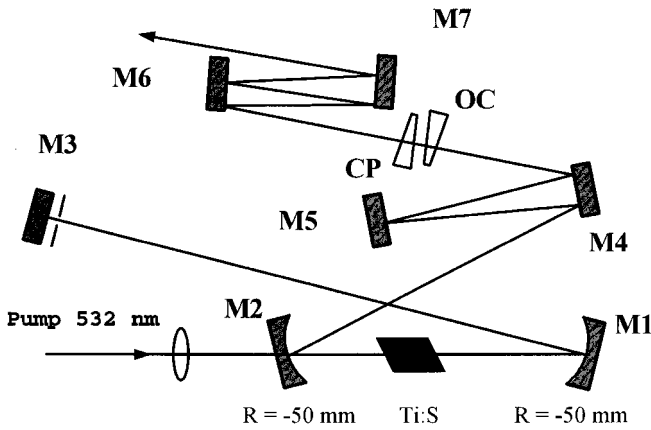


Fig. 20. Schematic laser setup of a mirror-dispersion-controlled KLM Ti:S laser [68]

As an example, we present the measured GDD versus wavelength functions of some chirped mirror pieces used to build a MDC Ti:S laser pumped by a Millennia (Spectra-Physics, Inc.) laser at the Advanced Photon Research Center of the Japan Atomic Energy Research Institute (Ibaraki, Japan) [68]. Figure 20 illustrates the schematic laser setup. The laser exhibits a standard linear cavity [64, 65] comprising a 2.1 mm long (optical path) Ti:S crystal (Crystal Systems, $\alpha = 6 \text{ cm}^{-1}$) whose dispersion is compensated by seven reflections from chirped mirrors in one round-trip. M1 and M2 are standard quarterwave mirrors that are transparent for the pump wavelength (alternatively, these pump mirrors can be replaced by curved chirped mirrors since these too are transparent for the pump wavelengths and have similar dispersive properties to those of the flat chirped mirrors). Measured GDD functions of the chirped mirror pieces are plotted in Fig. 21. We use four reflections from mirror M4 (dotted curve), two reflections from M5, and one reflection from M3. The overall GDD originating from these chirped mirrors is also plotted in Fig. 21 (continuous line). It is seen that the overall GDD of the chirped mirrors is a nearly constant function from 740 to 860 nm, i.e., by measuring the GDD vs. wavelength functions of each chirped mirror piece after the

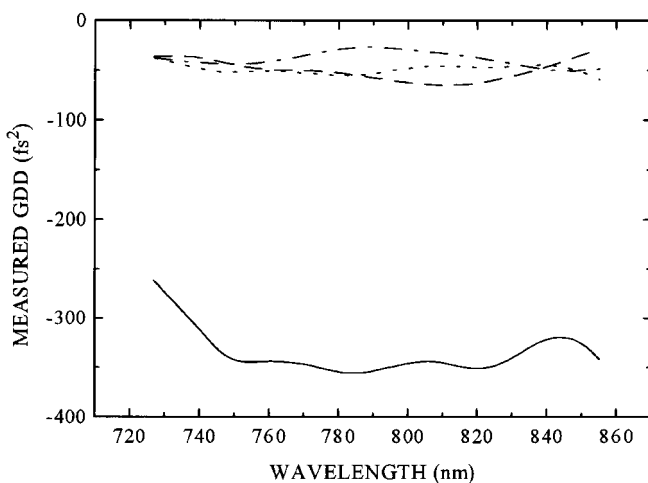


Fig. 21. Measured GDD vs. wavelength functions of the chirped mirror pieces used for building the sub-10-fs Ti:S oscillator shown in Fig. 20

deposition with high accuracy, and by proper selection of the mirrors, it is possible to realize a nearly optimum GDD vs. wavelength function for most of the application problems mentioned above [23–25, 35, 36, 64, 65, 68].

2.5 Defining the target function for different application problems

Let us continue dealing with the design of *chirped mirrors developed for modelocked femtosecond pulse solid-state laser oscillators and parametric oscillators, when chirped mirrors provide exclusively the negative dispersion in these cavities*, i.e., we continue our treatment with mirror-dispersion-controlled oscillators [23, 24, 26, 27, 29, 56, 64, 65].

2.5.1 Low-loss chirped mirrors for a sub-20-fs Cr:LiSAF and Cr:LiSGaF lasers.

In order to design a compact laser set-up comprising only chirped mirrors for intracavity dispersion compensation [27, 56], precise knowledge is required of the dispersion data not only of the dispersive mirrors [38, 39] but also of the laser active materials utilized. During our studies, however, we were unable to find dispersion data on some laser-active materials, e.g., Cr:LiSGaF; alternatively, the dispersion data we found in the literature did not fit our measured data in some other cases, e.g., in the case of the Cr:LiSAF crystal. Moreover, we observed strong dependence of the measured GDD on the doping concentration and/or the supplier of the crystal [69]. We mention the striking situation we faced when we started dealing with *modelocked MDC Cr:LiSAF lasers*. In Fig. 22, measured GDD vs. wavelength functions are plotted for 10-mm long LiSAF crystals with different Cr doping concentrations: (i) 0.8% (Lightning Optical Corporation), (ii) 2.0% (Strathclyde University, Glasgow). The crystal dispersion was measured at the Brewster angle for extraordinary rays by the method described in detail in [69]. It can be seen that the measured GDD vs. wavelength function considerably depends on the doping concentrations.

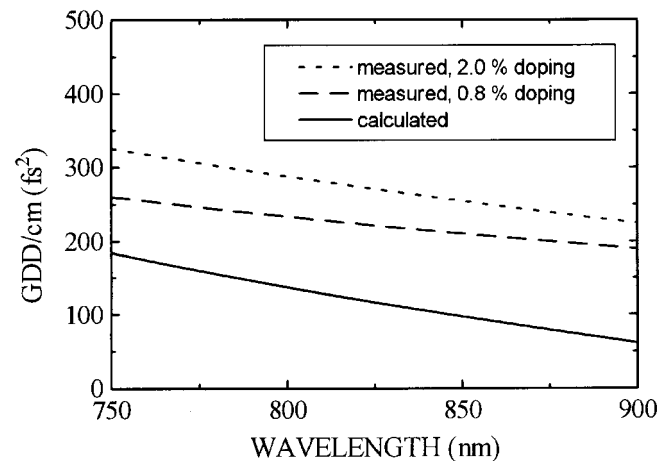


Fig. 22. GDD vs. wavelength functions plotted for 2-mm by 5-mm long LiSAF crystals with different Cr doping concentrations: (i) 0.8% (Lightning Optical Corporation), (ii) 2.0% (Strathclyde University, Glasgow). Dispersion of the crystals was measured at the Brewster angle for extraordinary rays. The calculated values correspond to the Sellmeier formula (see [3])

This dependence could also be derived from the Kramers–Kronig relation. For comparative purposes, the calculated GDD values corresponding to the Sellmeier formula presented in [3] are plotted as well. Since the pulse duration of mode-locked solid-state lasers depends strongly on the intracavity overall negative GDD, which is related to their soliton-like pulse-shaping mechanism, the number of reflections from the chirped mirrors and their nominal GDD/reflection value have to be chosen in accordance with the actual dispersion of other intracavity elements such as the laser active medium [27]. Accordingly, the target function defined by (31) must be derived as

$$D_{\text{GDD,OPT}}(\lambda_j) = \frac{-(D_{\text{GDD,MEAS}}(\lambda_j) + |\Delta D_{\text{GDD,RES}}|)}{m}, \quad (33)$$

where m is the (integer) number of reflections from chirped mirrors in the cavity per round-trip, $D_{\text{GDD,MEAS}}(\lambda_j)$ is the measured overall (positive) GDD vs. wavelength function of other cavity elements, and $\Delta D_{\text{GDD,RES}}$ is the absolute value of the optimum overall (negative) GDD for mode-locked operation.

With precise information on the dispersion of Cr:LiSAF and Cr:LiSGaF crystals obtained by measuring their phase shift vs. wavelength functions in the frequency domain [69], we were able to construct compact MDC laser oscillators delivering sub-20-fs pulses directly from the laser oscillators [27], which are suitable for direct diode pumping.

When defining the search space and the target function, an additional important technological issue is the reflection losses on the chirped mirrors. In a diode pumped, mode-locked fs solid-state laser, the reduction of the reflection losses in the cavity is of primary importance. Let us recall that the optical quality of substrates is described by the rms (root-mean-square) roughness (σ). According to [70] (and assuming a wavelength-independent reflection delay of $\tau = 1$ fs), the reflection losses (ΔR_σ) of high reflectors corresponding to a rms surface roughness σ can be described by the following formula at wavelength λ :

$$\Delta R_\sigma(\lambda) = \left(\frac{4\pi\sigma}{\lambda} \right)^2. \quad (34)$$

The results of (34) are the following. (i) The scattering losses decrease towards the longer wavelengths. (ii) A lower surface roughness (originating from the higher quality of the substrates or from the higher density of the deposited layers) reduces the scattering losses. In connection with (i), we recall that in chirped dielectric mirrors intended for intracavity use, the group-delay increases towards the longer wavelengths. Furthermore, it was shown in [14] that *in dielectric high reflectors, reflection losses are proportional to the reflection delay* at a certain wavelength when the same coating materials and deposition technology are used for each reflector. Accordingly, the wavelength-dependent reflection losses at chirped (or any other dispersive) mirrors can be written as

$$\Delta R(\lambda) = \Delta R_\sigma(\lambda) \tau(\lambda). \quad (35)$$

As a result, reflection losses at chirped mirrors can be minimized by (i) reducing the surface roughness (σ) of the chirped mirrors and (ii) reducing the maximum value of the

reflection delay. The first possibility was experimentally tested by depositing dielectric high reflectors with different coating materials and deposition technologies, the result of which is demonstrated in Fig. 23a,b. *By properly choosing the substrates, the coating materials and the technology for coating deposition, we were able to considerably decrease the surface roughness of our mirrors.* Further technical details on the coating deposition technology are available in [14]. The maximum value of the GDD vs. wavelength function is traded off against the bandwidth of the mirror, as follows from the definition of the GDD:

$$D_{\text{GDD}} = \frac{d\tau}{d\omega} \cong \frac{\Delta\tau}{\Delta\omega}. \quad (36)$$

In other words, a certain amount of positive $D_{\text{GDD,MEAS}}$ in the cavity [see (33)] calls for a minimum negative GDD originating from the chirped (or Gires–Tournois [26]) dielectric mirrors for dispersion compensation. The reflection losses at

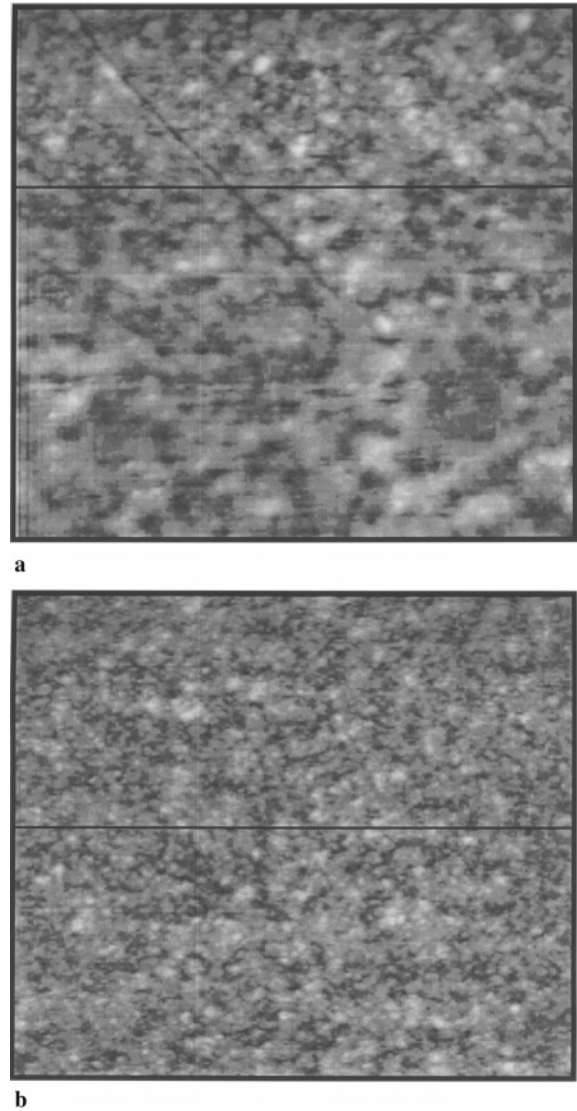


Fig. 23a,b. Atomic Force Microscopy measurements on chirped laser mirrors using different coating materials and technologies for coating deposition. The lower grain size results in lower scattering losses of the mirrors

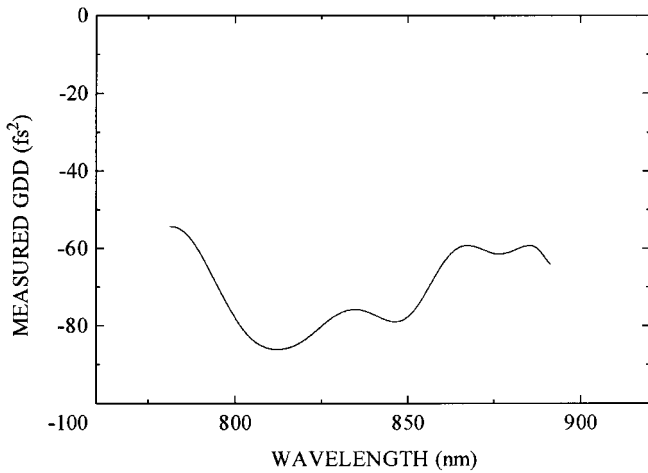


Fig. 24. Measured GDD vs. wavelength function of chirped mirrors designed for sub-20-fs Cr:LiSAF and Cr:LiSGaF lasers [27]

the mirrors, however, can be reduced by reducing the overall group delay on reflection, which can be minimized at the expense of the reduced bandwidth ($\Delta\omega$). For the experiment described in [27], chirped mirrors exhibiting a GDD per reflection of $\cong -80 \text{ fs}^2$ from 800 to 900 nm were constructed. The measured GDD vs. wavelength function of the mirrors is shown in Fig. 24. Both of our Cr:LiSAF and Cr:LiSGaF lasers both delivered sub-20-fs pulses from an extremely compact mirror-dispersion-controlled cavity capable of direct diode pumping [27].

2.5.2 Ultra-broadband chirped mirrors for broadly tunable femtosecond Ti:S lasers and pulse compression experiments. One of the main practical complication factors in connection with using broadly tunable cw, ps and fs laser systems is the lack of ultra-broadband, low-loss dielectric high reflectors for feedback in these systems. Fluorescence bands of broadband laser active materials such as Ti:S [1] are usually covered by several low dispersion quarterwave mirror sets that must be replaced when these lasers are tuned out of the (relatively narrow) reflectance band, which complicates the practical application of these or similar laser systems, such as OPOs.

Recently, we succeeded in solving the problem by developing ultra-broadband chirped mirrors (UBCM) for a broadly tunable cw and ultrafast Ti:S laser [28]. The main difference during its design compared to previous designs was that we required a high transmittance at the pump wavelengths, i.e., $R_{\text{OPT}}(\lambda_j) = 0$ in (30), and we allowed a higher tolerance in (31).

Figure 25 shows the calculated transmittance of one of our present state-of-the-art UBCMs. A high reflectivity ($R > 99\%$) from 660 to 1060 nm was obtained for normal incidence by computer optimization that covers most of the fluorescence band of the Ti:S. The mirrors are designed for high transmission ($T > 90\%$) at the pump wavelengths of 488 and 514 nm in order to test the UBCMs in a fs Ti:S laser system (Coherent MIRA 900) pumped by a multiline 8.0 W Ar⁺-laser (Coherent Innova 400).

This specific design is built up of alternating layers of SiO₂ and TiO₂ as the low- and high-index materials, respectively, with optical thicknesses varying around a quarter of 800 nm, corresponding to our selected wavelength regime.

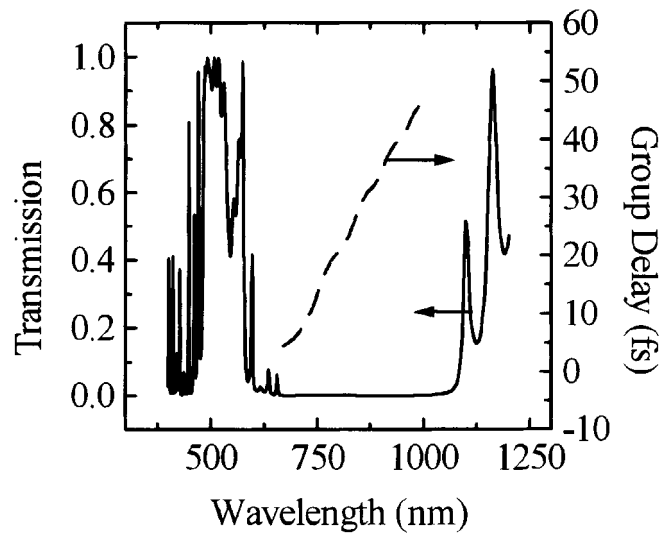


Fig. 25. Transmittance (solid line) and group delay (dashed line) of an ultra broadband CM vs. wavelength. Optical thickness coefficients of the design are [71]:

S | 1.31L 1.70H 1.43L 0.66H 1.55L 1.45H 1.04L 1.20H 1.14L 1.32H 1.47L 0.99H 0.97L 1.17H 1.46L 1.15H 1.18L 1.11H 1.09L 1.08H 1.11L 1.33H 1.19L 0.91H 1.11L 0.96H 1.05L 0.83H 0.93L 1.11H 1.01L 0.98H 0.85L 0.90H 0.79L 0.99H 0.80L 0.93H 0.96L 0.60H 0.69L 1.09H 0.97L 0.41H 0.59L 1.35H 0.90L 0.10H | A.

S: substrate, $n_S = 1.51$; A: air, $n_A = 1.0$; H and L: quarterwave layers of TiO₂ and SiO₂, respectively, at $\lambda = 790 \text{ nm}$, $n_H = 2.315$, $n_L = 1.45$

The Optical thickness coefficients of the design are listed in the figure caption [71]. The theoretical smooth variation of group delay vs. frequency of the UBCM's is plotted in Fig. 25. We verified the dispersive properties of the chirped mirror coatings after the deposition process by using the white-light interferometric technique described in [38]. These mirrors were designed to have an average negative GDD of -50 fs^2 and a positive TOD of $+75 \text{ fs}^3$ around 800 nm to ensure nearly ideal dispersive conditions for mode-locked operation. The considerable extension of the high reflectivity range of the CMs was achieved at the expense of a slightly higher fluctuation in the negative GDD, which, however, does not affect the formation of pulses longer than 50 fs.

In order to demonstrate the performance of the UBCMs, we replaced all mirrors, except the output coupler (OC) but including the dichroic pump mirror, by UBCMs in our Ti:S laser. The Ti:S laser is continuously tunable from 681 to 1013 nm in cw operation with only one change of the output coupler (OC). The wavelength dependence of the cw output power is similar to the one in mode-locked operation (Fig. 26) with a maximum of 1.34 W at 770 nm. The wavelength range of cw operation agrees quite well with the calculated high-reflectivity range of the UBCMs.

Figure 26 shows the measured output power over the tuning range (693 nm to 975 nm) in mode-locked operation. The plotted output power was measured with the pulse duration kept constant at about 85 fs. In practice, we were not able to observe any decrease in the laser output power when using the UBCMs instead of $\lambda/4$ -stack standard type mirrors. The intracavity negative GDD required for mode-locked operation is provided by a standard Brewster-angled prism pair and the UBCMs. This hybrid solution is necessary since the negative GDD of practicable UBCMs is too low to compen-

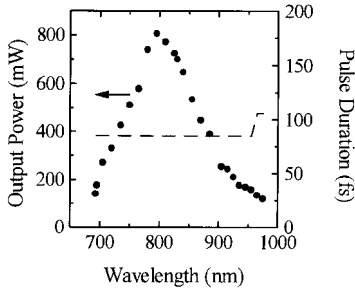


Fig. 26. Output power (dots) and pulse duration (dashed line) of the fs-Ti:sapphire laser using ultra-broadband chirped mirrors. For intracavity dispersion control, a standard Brewster-angled prism pair made of SF10 glass was used in a Coherent MIRA 900 laser with a prism separation of 60 cm [28]

sate for the positive material GDD of the 20-mm-long Ti:S crystal used in our laser setup. *The hybrid dispersion-control system combines the advantages of the CM approach, which allows higher-order dispersion compensation for relatively long crystals, and the continuous variation of the GDD by the prisms* [25].

Recent results show that in combination with prism pairs, the presented ultra-broadband chirped mirrors [28] with properly chosen third- and fourth-order dispersion functions are well suited for white-light continuum compression below 5 fs [35, 36].

In order to take an example for dispersion control up to the fourth order, we present the computed transmittance and group delay functions of an ultra-broadband chirped mirror design composed of three different layer materials in order to minimize reflection losses. The mirrors were required to be transparent around 532 nm and to have high reflectivity over most of the fluorescence band of Ti:sapphire. The computed transmittance vs. wavelength and group delay vs. wavelength functions are plotted in Figs. 27 and 28. The ultra-broadband chirped mirror exhibits negative GDD, positive TOD and positive FOD ($= \partial^4 \varphi / \partial \omega^4$) around 800 nm, as shown in the figure. Combination of such mirrors with prism pairs results in a nearly constant overall negative GDD in the laser cavity, or

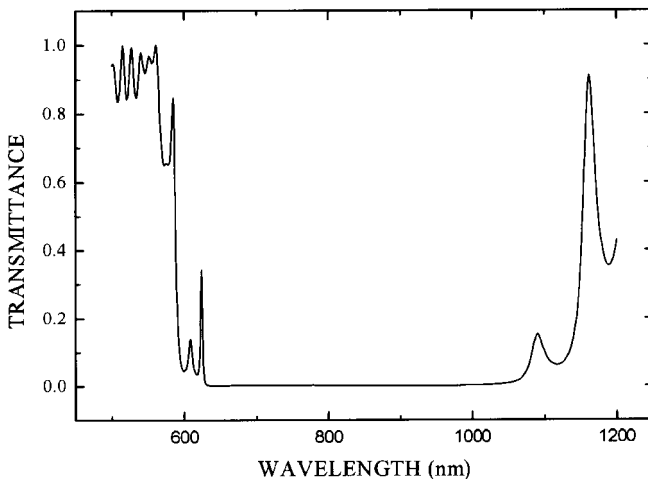


Fig. 27. Transmittance of a three-component ultra broadband CM vs. wavelength developed for a broadly tunable Ti:sapphire laser

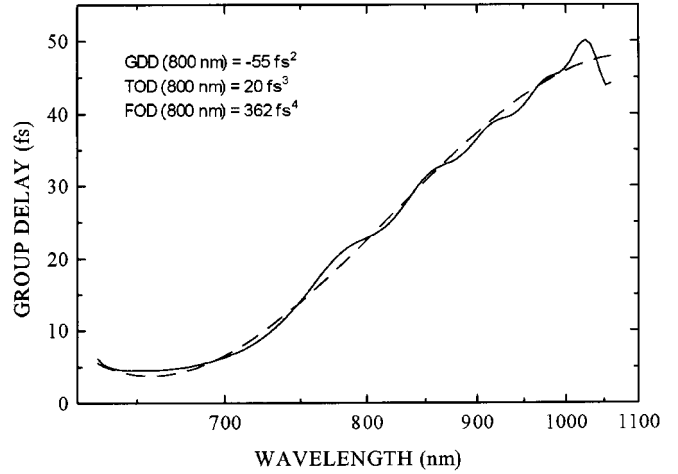


Fig. 28. Group delay of a three-component ultra broadband CM vs. wavelength developed for a broadly tunable Ti:sapphire laser

a nearly ideal group delay vs. wavelength functions in hybrid white-light-continuum compression schemes.

One can use all of the dielectric mirrors at oblique angles of incidence in extra-cavity broad spectrum laser applications, such as in pulse-compression schemes. It is well known from thin-film theory [13] that the effective refractive indices of the layers also depend on the angle of incidence and the polarization of light:

$$n_{s,\text{eff}} = n \cos \theta, \quad (37a)$$

$$n_{p,\text{eff}} = \frac{n}{\cos \theta}, \quad (37b)$$

where n and θ denote the refractive index of the i th layer and the angle of refraction in the i th layer, and n_s and n_p stand for the effective refractive indices for s- and p-polarized light, respectively. In effect, it results in broader reflectance bands and higher reflectivities for s-polarized light and narrower reflectance bands and lower reflectivities for p-polarized light in case of standard $\lambda/4$ stacks [13]. A recent study on broad-

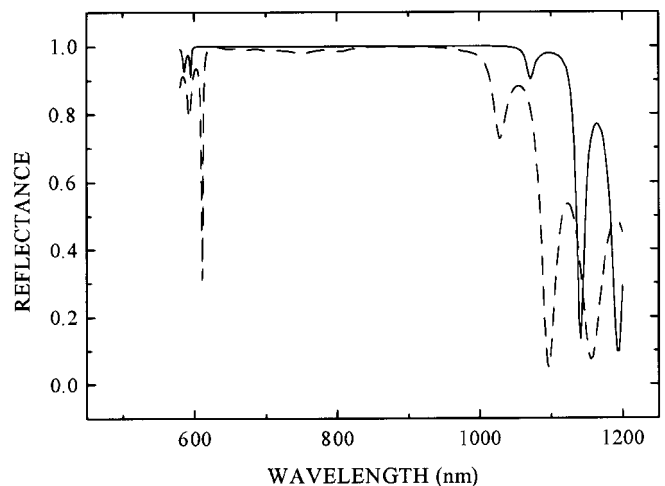


Fig. 29. Reflectance of a three-component ultrabroadband CM vs. wavelength computed for s-polarized light (continuous line) and p-polarized light (dashed line) at oblique incidence ($\theta = 45^\circ$)

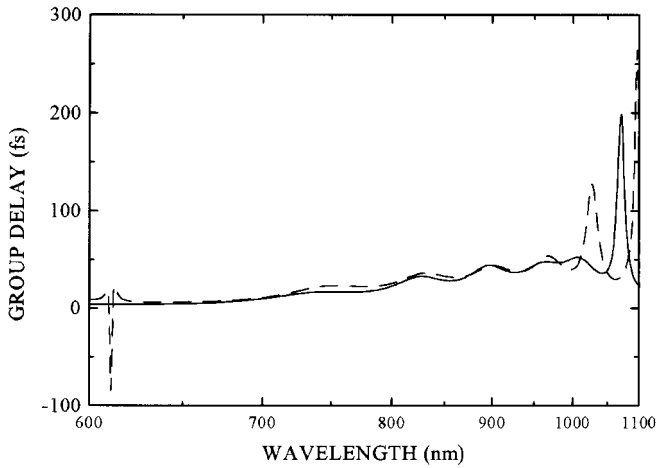


Fig. 30. Group delay of a three-component ultra broadband CM vs. wavelength computed for s-polarized light (continuous line) and p-polarized light (dashed line) at oblique incidence ($\theta = 45^\circ$)

band high-reflection multilayer coatings at oblique angles of incidence were recently published by Popov et al. [71]. In Figs. 29 and 30, we compare the reflectivity and group-delay vs. wavelength functions of the latest three-component design for s- and p-polarized light.

Comparing the reflectance bands, we find that the high-reflectivity range of the dielectric chirped mirror is extended for s-polarized light and reduced for p-polarized light, as with $\lambda/4$ stacks. With respect to the group delay vs. wavelength functions we find the following: the group delay exhibits a higher modulation for oblique incidence for both polarizations that must be a problem in pulse-compression experiments. During our previous studies, however, we found that this oscillation can be considerably reduced by computer optimization. Additionally, it is worth pointing out that the group delay and thus the reflection losses could take a lower value for s-polarized light, which might be important in intracavity applications.

2.5.3 Third- and fourth-order dispersion compensation by means of chirped dielectric laser mirrors in a sub-10-fs Ti:sapphire laser. In the previous section, we mentioned that *chirped mirrors exhibiting negative GDD, positive TOD, and positive FOD* [28, 33, 38] are suitable for balancing the TOD and FOD of laser cavities comprising prism pairs for intracavity dispersion control. In order to demonstrate the powerfulness of this combination, we present the recent results of Kärtner et al. [25], who worked with a self-starting, KLM Ti:sapphire laser comprising a prism pair in combination with some of our chirped mirrors for intracavity and extracavity dispersion control. Figure 31 shows the measured GDD versus wavelength function of the chirped mirror we provided for the experiment. According to his test results, the laser delivers approximately 7.4-fs pulses directly from the Ti:S oscillator, which competes with the best results obtained with the mirror-dispersion-controlled Ti:sapphire ring oscillator recently reported by Xu et al. [24]. The hybrid laser is pumped by a multi-line Ar-ion laser with an output power of 5.5 W. With a 3% output coupler, the mode-locked output power of the laser is 120 mW. The laser utilizes a broadband

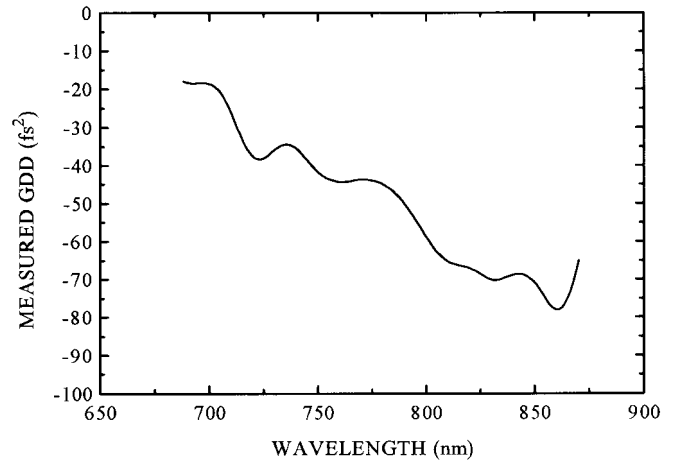


Fig. 31. Measured GDD vs. wavelength function of a chirped mirror manufactured for higher-order dispersion control in a self-starting, soft aperture KLM Ti:S laser delivering sub-10-fs pulses directly from the oscillator [25]

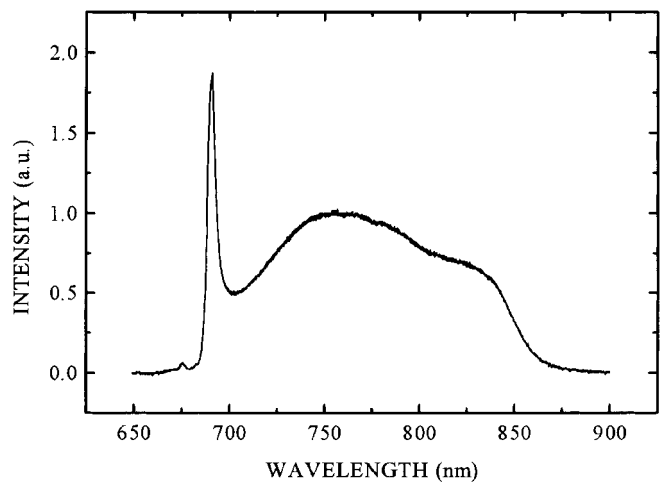


Fig. 32. Measured spectrum of a Ti:sapphire laser comprising a prism pair in combination with chirped mirrors for intra- and extracavity dispersion control

semiconductor saturable absorber mirror (SESAM) as a starting mechanism for soft-aperture KLM action. Besides the chirped mirrors with negative GDD and higher-order dispersion, a FS prism pair with prism separation of 41 cm was used for intracavity dispersion compensation of a 2.5-mm-long Ti:sapphire crystal. The bandwidth of the laser was limited by the finite bandwidth of the standard input couplers on the short wavelength side. It is worth pointing out that in this linear cavity the positive GDD (and positive TOD) introduced by the Ti:S crystal is approximately twice as much as that in the case of the ring oscillator developed by Xu et al. [24]. Nevertheless, this higher amount of positive TOD was efficiently compensated by balancing the negative TOD of the prism pair and the positive TOD of the chirped mirrors in this experiment. Figures 32 and 33 show the measured spectrum and interferometric autocorrelation traces of this Ti:S laser.

2.5.4 Chirped mirrors for an optical parametric oscillator working in the infrared. Continuing our work with fs OPOs employing chirped mirrors for intracavity dispersion compensation [29], recently we managed to manufacture *chirped*

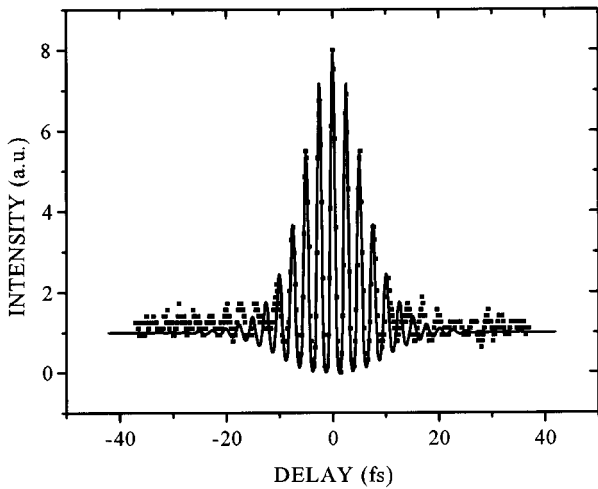


Fig. 33. Measured interferometric autocorrelation trace of the hybrid Ti:sapphire laser

mirrors with negative GDD and negative TOD [30]. The dispersive properties of the chirped mirrors were tailored to fit the dispersive properties of a 2-mm-long KTP crystal used for parametric wave generation. The wavelength dependence of the (absolute value of the) GDD of the KTP crystal and of the chirped mirror is shown in Fig. 34. The OPO is synchronously pumped by 130-fs to 170-fs pulses from a Coherent MIRA 900 Ti:sapphire laser. The OPO generates nearly transform limited 50 fs pulses with a time–bandwidth product below 0.5. Tuning of this device requires only the variation of the pump pulse wavelength and the cavity length. Over a tuning range of 100 nm, the pulse duration is less than half the pump pulse length [30].

Note added

After submission of this paper, two papers became available dealing with exact coupled-mode theory for multilayer interference coatings with arbitrary strong index modulations [72] and introducing “double” chirped mirrors [73]. Both papers

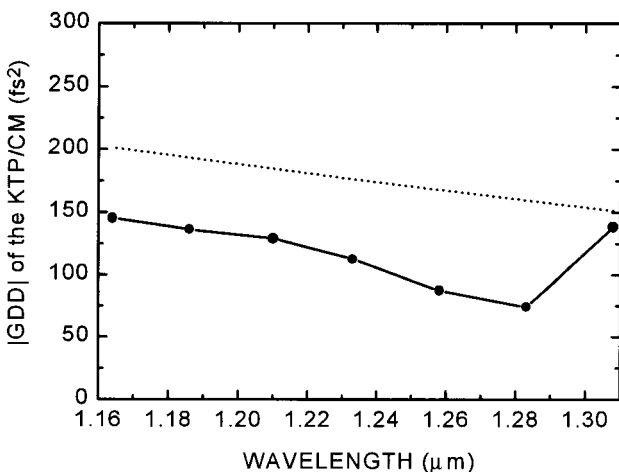


Fig. 34. Wavelength dependence of the absolute value of GDD of the KTP crystal and of the chirped mirror developed for an optical parametric oscillator working in the infrared spectrum [30]

present valuable results that might help in solving the problems originating from the approximate nature of the Fourier-transform method described in Sect. 1.3.

3 Conclusion

Chirped dielectric laser mirrors for broadband feedback, intracavity and extracavity dispersion control have been introduced. The design technique, deposition technology, and quality control permit higher-order contributions to the mirror phase dispersion to be kept at low values or to be chosen such that high-order phase errors introduced by other system components (e.g., the gain medium, prism pairs) are cancelled. By replacing conventional thin-film optics (and prism pairs in most of the cases) these novel devices made it feasible to build Kerr-lens mode-locked, all-solid-state lasers delivering nearly bandwidth-limited sub-10-fs pulses from Ti:sapphire lasers around 0.8 μm , and sub-20-fs pulses from Cr:LiSAF and Cr:LiSGaF lasers around 840 nm. Further applications of chirped mirrors that have been accomplished were discussed: for broadband feedback and dispersion control in broadly tunable cw, ps and fs solid-state lasers and parametric oscillators, broadband third-order (and fourth-order) dispersion control in pulse compression schemes used in CPA systems; or in white light continuum compression experiments supporting pulses below 5 fs. Basic theoretical and design considerations were also presented.

Acknowledgements. The authors thank K. Ferencz for manufacturing the mirrors used in the above mentioned experiments. Helpful discussions with P. Apai, A. Baltuska, Z. Bor, M. Danailov, J.A. Dobrowolski, K. Ferencz, J. Hebling, I. Jung, J. Kafka, F. Kartner, A. Kasper, U. Keller, D. Kopf, A.P. Kovács, F. Krausz, J. Kuhl, E. Mayer, J. Möbius, K. Osvay, M. Pschenichnikov, I. Sorokina, Ch. Spielmann, A. Stingl, V. Tikhonravov, P. Tourmois, P. Verly, L. Xu and E. Wintner are also gratefully acknowledged. We especially thank F. Krausz for directing our attention to the problems in connection with using conventional thin film optics in femtosecond pulse laser systems and helping us in the specification and testing of the first chirped mirrors, Z. Bor for helping our work with relevant references and advice in a number of cases, I. Jung for providing the data shown in Figs. 32 and 33, A.P. Kovács for performing the AFM measurements shown in Figs. 23a,b and for his help by all other means, and A. Baltuska for providing his preliminary test results, shown in Fig. 14. This research was supported by the OTKA Science Foundation of Hungary under grants CW-015285 and T-02056, the Hungarian State Eötvös Fellowship and by R&D Lézer-Optika Bt., Budapest, Hungary.

References

1. P.F. Moulton: *J. Opt. Soc. Am. B* **3**, 125 (1986)
2. B.W. Woods, S.A. Payne, J.E. Marion, R.S. Hughes, L.E. Davis: *J. Opt. Soc. Am. B* **8**, 970 (1991)
3. S.A. Payne, W.F. Krupke, L.K. Smith, W.L. Kway, L.D. DeLoach, J.B. Tassano: *IEEE J. Quantum Electron.* **28**, 1188 (1992)
4. L.K. Smith, S.A. Payne, W.L. Kway, L.L. Chase, B.H.T. Chai: *IEEE J. Quantum Electron.* **28**, 2612 (1992)
5. D. Kopf, J. Aus der Au, U. Keller, G.L. Bona, P. Röntgen: *Opt. Lett.* **20**, 1782 (1995)
6. R. Knappe, K.J. Boller, R. Wallenstein: *Opt. Lett.* **20**, 1988 (1995)
7. D.E. Spence, P.N. Kean, W. Sibbett: *Opt. Lett.* **16**, 42 (1991)
8. Ch. Spielmann, P.F. Curley, T. Brabec, F. Krausz: *IEEE J. Quantum Electron.* **30**, 1100 (1994)
9. R.L. Fork, O.E. Martinez, J.P. Gordon: *Opt. Lett.* **9**, 150 (1984)
10. P.F. Curley, Ch. Spielmann, T. Brabec, F. Krausz, E. Wintner, A.J. Schmidt: *Opt. Lett.* **18**, 54 (1993)
11. I.P. Christov, M.M. Murnane, H.C. Kapteyn, J. Zhou, C.P. Huang: *Opt. Lett.* **19**, 1465 (1994)

12. F. Abeles: "Recherches sur la propagation des ondes electromagnetiques sinusoidales dans les milieus stratifies", *Ann. Phys., Paris* 12th series, 5, pp. 596–640, and pp. 706–784 (1950)
13. H.A. Macleod: In *Thin Film Optical Filters* (Adam Hilger, Bristol 1985) Chap. 2
14. K. Ferencz, R. Szipöcs: *Opt. Eng.* **32**, 2525 (1993)
15. P.J. Martin: *J. Mat. Sci.* **21**, 1 (1986)
16. A.F. Turner, P.W. Baumeister: *Appl. Opt.* **5**, 69 (1966)
17. O.S. Heavens, H.M. Liddell: *Appl. Opt.* **5**, 373 (1966)
18. J. Ebert, H. Pannhorst, H. Küster, H. Welling: *Appl. Opt.* **18**, 818 (1979)
19. P. Laporta, V. Magni: *Appl. Opt.* **24**, 2014 (1985)
20. A.M. Weiner, J.G. Fujimoto, E.P. Ippen: *Opt. Lett.* **10**, 71 (1985)
21. R. Szipöcs, K. Ferencz, Ch. Spielmann, F. Krausz: *Opt. Lett.* **19**, 201 (1994)
22. R. Szipöcs, A. Kóházi-Kis: *Proc. SPIE* **2253**, 140 (1994)
23. A. Kasper, K.J. Witte: *Opt. Lett.* **21**, 360 (1996)
24. L. Xu, Ch. Spielmann, F. Krausz, R. Szipöcs: *Opt. Lett.* **21**, 1259 (1996)
25. I.D. Jung, F. Kärtner, N. Matuschek, D.H. Sutter, F. Morier-Genoud, Z. Shi, V. Scheuer, M. Tilsch, T. Tschudi, U. Keller: *Appl. Phys. B* **65**, 137 (1997)
26. I.T. Sorokina, E. Sorokin, E. Wintner, A. Cassanho, H.P. Jenssen, R. Szipöcs: *Opt. Lett.* **21**, 1165 (1996)
27. I.T. Sorokina, E. Sorokin, E. Wintner, A. Cassanho, H.P. Jenssen, R. Szipöcs: *Appl. Phys. B* **65**, 245 (1997)
28. E.J. Mayer, J. Möbius, A. Euteneuer, W.W. Rühle, R. Szipöcs: *Opt. Lett.* **22**, 528 (1997)
29. J. Hebling, E.J. Mayer, J. Kuhl, R. Szipöcs: *Opt. Lett.* **20**, 919 (1995)
30. J. Hebling, H. Giessen, S. Linden, J. Kuhl, "Mirror-dispersion-compensated femtosecond optical parametric oscillator", *Opt. Comm.*, in press
31. R.H. Lehmburg, U.S. Pat. No. 3,943,457 (1974)
32. D. Strickland, G. Mourou: *Opt. Comm.* **56**, 219 (1985)
33. Ch. Spielmann, M. Lenzner, F. Krausz, R. Szipöcs: *Opt. Comm.* **120**, 321 (1995)
34. R.L. Fork, C.H. Brito Cruz, P.C. Becker, C.V. Shank: *Opt. Lett.* **12**, 483 (1987)
35. A. Baltuska, Z. Wei, M.S. Pshenichnikov, D.A. Wiersma: *Opt. Lett.* **22**, 102 (1997), and A. Baltuska, Z. Wei, R. Szipöcs, M.S. Pshenichnikov, D.A. Wiersma: *Appl. Phys. B* **65**, 175 (1997)
36. M. Nisoli, S. De Silvestri, O. Svelto, R. Szipöcs, K. Ferencz, S. Sartania, Ch. Spielmann, F. Krausz: *Opt. Lett.* **22**, 522 (1997), and M. Nisoli, S. Stagira, S. De Silvestri, O. Svelto, S. Sartania, Z. Cheng, M. Lenzner, Ch. Spielmann, F. Krausz: *Appl. Phys. B* **65**, 189 (1997)
37. Yu.T. Mazurenko: *Appl. Phys. B* **50**, 101 (1990)
38. A.P. Kovács, K. Osvay, Z. Bor, R. Szipöcs: *Opt. Lett.* **20**, 788 (1995)
39. K. Osvay, G. Kurdi, J. Hebling, A.P. Kovács, Z. Bor, R. Szipöcs: *Opt. Lett.* **20**, 2339 (1995)
40. B. Loiseaux, A. Delboulbe, J.P. Huignard, P. Tournois, G. Cheriaux, F. Salin: *Opt. Lett.* **21**, 806 (1996)
41. K.B. Hill, D.J. Brady: *Opt. Lett.* **18**, 1739 (1993)
42. A.M. Weiner, D.E. Leaird, D.H. Reitze, E.G. Paek: *IEEE J. Quantum Electron.* **28**, 2251 (1992)
43. M.B. Danailov, K. Diomande, P. Apai, R. Szipöcs: "Phase conjugation of broadband laser pulses in BaTiO₃", *J. Mod. Opt.* in press
44. L. Sossi, P. Kard: *Eesti NSV Tead. Akad. Toim. Fuss. Mat.* **17**, 41 (1968) (An English translation of this paper is available from the Translation Services of the Canada Institute for Scientific and Technical Information, National Research Council, Ottawa, Ontario K1A 0S2, Canada.)
45. L. Sossi: *Eesti NSV Tead. Akad. Toim. Fuss. Mat.* **23**, 229 (1974)
46. L. Sossi: *Eesti NSV Tead. Akad. Toim. Fuss. Mat.* **25**, 171 (1976)
47. J.A. Dobrowolski, D. Lowe: *Appl. Opt.* **17**, 3039 (1978)
48. P.G. Verly, J.A. Dobrowolski: *Appl. Opt.* **29**, 3672 (1990)
49. H. Fabricius: *Appl. Opt.* **31**, 5191 (1992)
50. R.R. Willey: *Appl. Opt.* **32**, 2963 (1993)
51. B.G. Bovard: *Appl. Opt.* **32**, 5427 (1993)
52. A.V. Tikhonravov: *Appl. Opt.* **32**, 5417 (1993)
53. J. Drussel, J. Grantham, P. Haaland: *Opt. Lett.* **18**, 1583 (1993)
54. W.H. Southwell: *Appl. Opt.* **24**, 457 (1985)
55. H. Fabricius: *Appl. Opt.* **31**, 5216 (1992)
56. "Chirped dispersive dielectric mirror", U.S. Pat. No. 08/289,086, Inventors: R. Szipöcs (70%), F. Krausz (30%) (1993)
57. W.H. Southwell: *Appl. Opt.* **28**, 5091 (1989)
58. P. Tournois, P. Hartemann: *Opt. Comm.* **119**, 569 (1995)
59. W.H. Southwell, R.L. Hall: *Appl. Opt.* **28**, 2949 (1989)
60. J.A. Dobrowolsky, R.A. Kemp: *Appl. Opt.* **29**, 2879 (1990)
61. S. Kirkpatrick, C.D. Gelatt, M.P. Vecchi: *Science* **220**, 671 (1983)
62. C.P. Chang, Y.H. Lee, S.Y. Wu: *Opt. Lett.* **15**, 595 (1990)
63. S. Martin, J. Rivory, M. Schönauer: *Appl. Opt.* **34**, 2247 (1995)
64. A. Stingl, Ch. Spielmann, F. Krausz, R. Szipöcs: *Opt. Lett.* **19**, 204 (1994)
65. A. Stingl, M. Lenzner, Ch. Spielmann, F. Krausz, R. Szipöcs: *Opt. Lett.* **20**, 602 (1995)
66. J.A. Apfel: *Appl. Opt.* **15**, 2339 (1976)
67. H. Greiner: *Proc. SPIE* **2253**, 150 (1994)
68. K. Yamakawa, M. Aoyama, T. Itoh, Ch. Spielmann: *Jpn. J. Appl. Phys.* **35**, L-989 (1996)
69. R. Szipöcs, A.P. Kovács, Z. Bor, "Dispersion Measurement on Crystals for ultrashort pulse generation using interference in the frequency domain", Conference on Lasers and Electro-Optics (Baltimore 1997) Paper CTuP32
70. H.E. Benett, J.M. Benett, In *Physics of Thin Films*, Academic Press, New York (1967)
71. K.V. Popov, J.A. Dobrowolski, A.V. Tikhonravov, B.T. Sullivan: *Appl. Opt.* **36**, 2139 (1997)
72. N. Matuschek, F. Kartner, U. Keller: *IEEE J. QE* **33**, 295 (1997)
73. F. Kartner, N. Matuschek, T. Schibli, U. Keller, H.A. Haus, C. Heine, R. Morf, V. Scheuer, M. Tilsch, T. Tschudi: *Opt. Lett.* **22**, 831 (1997)